Complex Seismic Anisotropy beneath Germany from *KS Shear Wave Splitting and Anisotropic Receiver Function Analysis

Leah Campbell

Adviser: Maureen Long
Second Reader: Jeffrey Park

April 29, 2015

A Senior Essay presented to the faculty of the Department of Geology and Geophysics, Yale University, in partial fulfillment of the Bachelor's Degree.

CONTENTS

ABSTRACT

Seismic anisotropy beneath stable continental interiors likely reflects a host of processes, including deformation in the lower crust, frozen anisotropy from past deformation events in the lithospheric mantle, and present-day mantle flow in the asthenosphere. Because the anisotropic structure beneath continental interiors is generally complicated and often exhibits heterogeneity both laterally and with depth, a complete characterization of anisotropy and its interpretation in terms of deformational processes is challenging. In this study, we aim to expand our understanding of continental anisotropy by characterizing in detail the geometry and strength of azimuthal anisotropy beneath Germany and the surrounding region, using a combination of shear wave splitting and receiver function analysis. We utilize data from ten long-running broadband stations in and around Germany, collected from a variety of national and temporary European networks. We measure the splitting of SKS, SKKS, and PKS phases, with the aim of obtaining the best possible backazimuthal coverage. Our results indicate that anisotropy beneath Germany is generally complex and cannot be adequately characterized by previously suggested simple models. We observe shear wave splitting patterns that are complicated and inconsistent with a single horizontal layer of anisotropy beneath the station. Observed delay times vary dramatically between stations from 0.7-2.3s and there is a preponderance of null *KS arrivals in the dataset, with null measurements detected over a fairly large swath of backazimuths. Although we note backazimuthal variations in splitting at several stations, we do not observe a clear 90-degree periodicity that one would expect for the case of multiple anisotropic layers. Transverse component receiver function analysis reveals evidence for dipping interfaces and possible non-horizontal anisotropic layers within the mantle lithosphere, providing further indicators of the complexity of anisotropy in this region. In the context of surface geological features and the localized deformation history, our results suggest that there are contributions to anisotropy at different depths with a variety of causes, including both fossilized anisotropy from past tectonic events and modern-day asthenospheric flow.

1 INTRODUCTION

Despite the simplifications made in early Earth models, it has long been recognized that Earth's interior is not only highly heterogeneous but also anisotropic. Anisotropy is a property of elastic materials by which the velocity of seismic waves is dependent on their propagation direction or polarization (Long and Becker, 2010). The discovery of anisotropy in large parts of the crust, the upper mantle down to depths of 300-500km, the transition zone between 660 and 900km, and the D" layer at the core mantle boundary (CMB), has been used to explain the splitting of shear waves and normal modes, the azimuthal variations of head wave velocity, and discrepancies between Rayleigh and Love surface waves (Montagner and Guillot, 2002). Since the 1960s, there has been a concerted effort among seismologists to understand the underlying causes and extent of seismic anisotropy and determine how it relates to convective mantle flow and surface geology (Fouch and Rondenay, 2006).

On a first order analysis, anisotropy can be intrinsic or effective. In the first case, a solid body can be anisotropic to the microscopic scale as a result of the material's elastic properties. In the second case, anisotropy is structural, due to the layering of material with strong velocity contrasts, the preferred orientation of naturally anisotropic minerals, or the alignment of fractures and fissures in an otherwise isotropic medium (Bormann et al., 1996). The two major causes of effective anisotropy are termed shape (SPO) or lattice (LPO) preferred orientation. SPO can be thought of as the alignment of heterogeneities with contrasting elastic properties such as cracks or melt lenses, while LPO, which is considered more common in the mantle, is the statistical alignment of actual mineral grains due to plastic deformation in the dislocation creep regime (Montagner and Guillot, 2002).

Because anisotropy in the mantle results from deformation, a qualitative and quantitative analysis of anisotropy is one of the best tools for understanding the geometry of deformation at depth (Park and Levin, 2002; Long and Silver, 2009; Long and Becker, 2010). Laboratory experiments and the examination of mantle-derived rocks have helped to elucidate the relationships between deformation and the resulting anisotropy, particularly for olivine, the most common upper mantle mineral (e.g. Karato et al., 2008). However, this picture is complicated by

a variety of factors including type of shear, temperature, and total strain. Measuring anisotropy in the mantle can be useful for elucidating patterns of mantle flow, coupling between the lithosphere and the asthenosphere, and the mantle's role in plate tectonics (Park and Levin, 2002; Fouch and Rondenay, 2006). Importantly, anisotropy can be used to investigate both present day asthenospheric flow and past deformation events, which can be frozen in the lithospheric mantle as 'fossilized' anisotropy (Silver and Chan, 1988). Large scale studies indicate extensive lateral and vertical heterogeneities in anisotropy, which can be interpreted as transitions from present-day convective flow to frozen-in anisotropy, or the layering of successive deformation events at different depths (Becker et al., 2012). Despite advances in our understanding of mantle flow and anisotropy, these transitions are poorly understood and many questions remain regarding the relationship of anisotropy to mantle flow processes at depth and the geometry of flow in different tectonic regions (Long and Silver, 2009).

A thorough understanding of anisotropy beneath continental interiors is particularly useful for understanding the basic structures of continents and the complexities of orogenesis and continental collision, as well as the role of the mantle in these processes (Montanger and Guillot, 2002; Long and Silver, 2009). However, studying anisotropy beneath continental plates has proven to be far more challenging than under ocean basins, in part because continents are older and contain a far more complex assemblage of tectonic units, resulting in strong spatial variability and shorter length scales of coherent deformation (Silver and Chan, 1988; Silver and Chan, 1991; Babuska et al., 1993; Fouch and Rondenay, 2006; Long and Silver, 2009). On top of this, there is the added complexity that there may be strong contributions to anisotropy from both the lithosphere and the asthenosphere and, potentially, coupling between those two layers, which is not easily explained by plate tectonic theory (Silver, 1996). In general, studies suggest that stable continental regions contain anisotropy in both the lithosphere and sublithospheric mantle to depths of at least 200km. In many regions, anisotropy is closely related to surface geology, though in others anisotropy is more closely related to the local direction of absolute plate motion (Fouch and Rondenay, 2006). These observations suggest that tectonic plates are partially coupled to the underlying mantle and that anisotropy can be generated by mantle flow or fossilized deformation from past tectonic events, or a combination of the two (Park and Levin, 2002; Fouch and Rondenay, 2006). Because of the uncertainties that remain and the variability in

observations for different regions, a thorough and precise characterization of anisotropy in continents is crucial to understanding craton formation and other tectonic processes, as well as the vertical coherence of deformation between different layers of the mantle (Long and Becker, 2010).

The past few decades have seen the introduction of a variety of new techniques that have helped constrain continental anisotropy and thus allowed for a more precise characterization of mantle deformation. These techniques include shear wave splitting, receiver functions, and surface wave tomography, which can all help detect variations in anisotropy, laterally and vertically (Fouch and Rondenay, 2006). Because each technique has inherent limitations and can only be used to image a portion of the anisotropic structure, the most robust characterization of anisotropy can only be achieved by integrating different data sets and utilizing a variety of techniques. Incorporation of different sources of data allows for a more thorough interpretation of the type and origins of plate motion and how it relates to localized tectonic processes (Fouch and Rondenay, 2006; Long and Becker, 2010).

Shear wave splitting, the process by which a shear wave sampling an anisotropic layer will split into two orthogonal waves with distinct polarizations in a fast (φ) and slow direction, can provide some of the most direct constraints on anisotropic orientation and mantle flow and is thus one of the most popular methods (Park and Levin, 2002; Long and Silver, 2009). As the fast and slow quasi-S waves travel through the anisotropic layer, they accumulate a delay time, which, along with the polarization of the fast direction, contains information about the geometry and strength of anisotropy (Long and Becker, 2010). Because the observed splitting parameters integrate the effects of anisotropy along their entire path, shear wave splitting offers poor depth resolution (Silver and Chan, 1991). However, the study of the splitting of SKS waves in particular is extremely useful because 1) the initial polarization is controlled by the P to S conversion at the CMB and is thus known and 2) the SKS ray path is nearly vertical and thus it provides excellent lateral resolution (Marone and Romanowicz, 2007; Long and Becker, 2010).

Receiver function analysis relies on the partial conversion of compressional P-waves to shear S-waves at discontinuities to image the vertical layering of anisotropy and the orientation of

layered structures in the crust and upper mantle. This technique provides significant vertical, but poor horizontal resolution (Park and Levin, 2002; Fouch and Rondenay, 2006). Meanwhile, surface wave analysis considers the discrepancies in velocity between surfaces waves with different polarizations (ie. vertical for Rayleigh and horizontal for Love waves), as well as the behavior of waves with different propagation directions. It is a useful complement to the other techniques because it utilizes substantially longer wavelengths. Furthermore, the dispersive nature of surface waves means that surface waves can help resolve the depth distribution of anisotropy. (Long and Becker, 2010).

This study utilizes each of the above-mentioned techniques, in part to evaluate their strengths and limitations in reference to one another, but more importantly to contribute to the ongoing discussion of anisotropy in stable continental interiors, in particular beneath Germany. We have analyzed *KS splitting patterns for ten broadband seismic stations from different networks in and around Germany, acquiring data from as far back as thirty years (Figure 1).

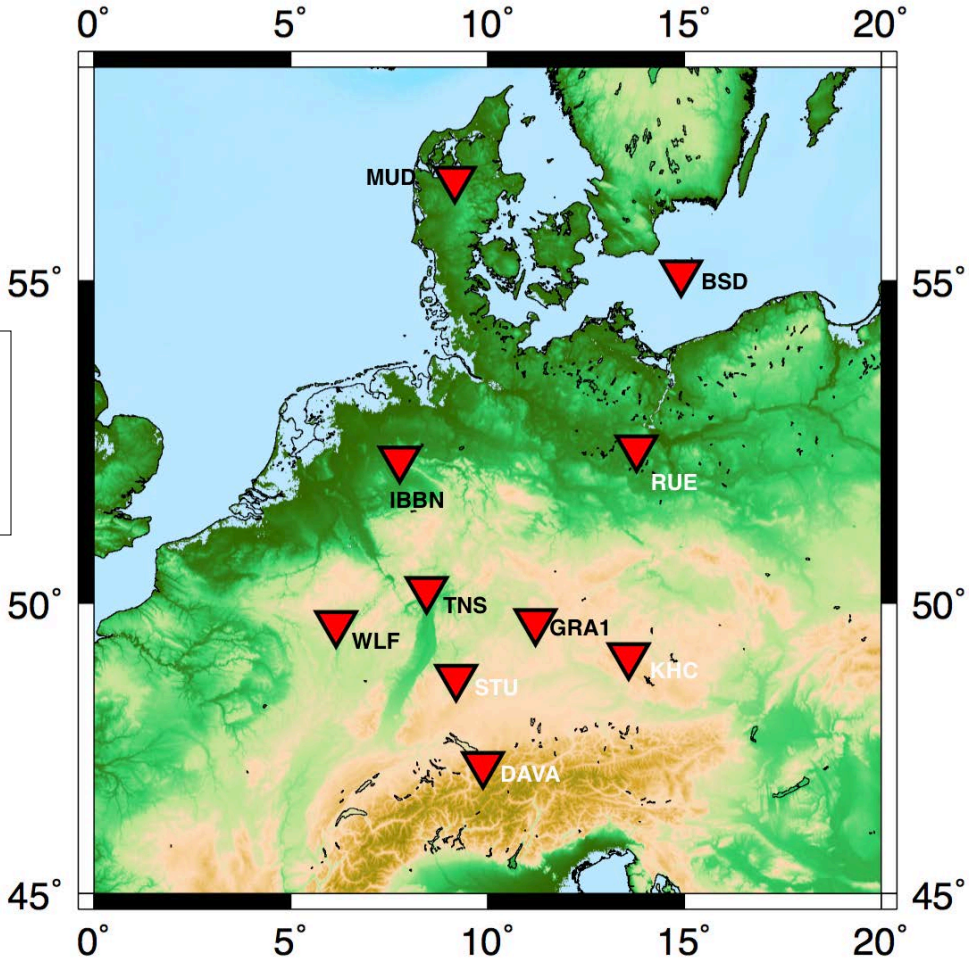

Fig. 1: Map of stations analyzed for shear wave splitting. Those written in white were also used in the receiver function analysis.

We have supplemented these measurements by generating radial and transverse receiver functions for four of those stations, shown in white in Figure 1, and comparing the results to previously-published regional and global surface wave models. At most stations we observe dramatic variations in *KS splitting with event backazimuth, suggesting lateral and/or depth variability of anisotropy. We also observe drastic changes in anisotropic parameters between adjacent stations. Transverse component receiver functions exhibit variations with backazimuth that suggest multiple layers of anisotropy with depth. While the results of our receiver function analysis generally agrees with our splitting measurements, there are distinct discrepancies between our results and those predicted by the surface wave models. These observations allow us to conclude that anisotropy underneath Germany is vastly complex, possibly multilayered and non-horizontal, with strong heterogeneities both laterally and vertically. While there is some correlation with surface geological features, the anisotropy in this region clearly cannot be explained simply by a single pattern or model of deformation.

2 BACKGROUND

2.1 Mechanisms of Anisotropy

The causes of anisotropy can be broadly categorized as shape preferred (SPO) versus lattice preferred (LPO) orientation mechanisms. SPO is the spatial organization of isotropic material with contrasting elastic properties (Montagner and Guillot, 2002). In the crust, SPO can be generated by structural alignments such as the preferred orientation of fluid-filled fractures and folds. In the mantle, SPO can come from melt-filled cracks or lenses. This process may be a significant cause of anisotropy directly beneath mid-ocean ridges and perhaps subduction zones (Fouch and Rondenay, 2006). In contrast, LPO is the process of reorienting, via deformation, the crystal lattices of intrinsically anisotropic minerals, such as olivine (Montanger and Guillot, 2002). Olivine, the main constituent of the mantle, is highly anisotropic, producing a difference in S-wave velocity between the fast and slow axis of anywhere from 7-12% (Nicolas and Christensen, 1987; Iturrino et al., 1991). Thus, the LPO of olivine is considered one of the predominant causes of anisotropy in the upper mantle (Montanger and Guillot, 2002; Karato et al., 2008). In the asthenosphere, where brittle fracturing is impossible, anisotropy is generally attributed to the LPO of olivine and pyroxene, aligned in the direction of upper mantle flow (Bormann et al., 1996).

Though both SPO and LPO are products of tectonic forces, they can yield conflicting anisotropic signals in response to the same stress field. For example, crustal SPO developed from cracks orthogonal to the direction of maximum stress, would produce an anisotropic fast polarization parallel to the long axis of the fractures, and thus perpendicular to the direction of maximum extension. In contrast, LPO due to olivine deformation in the mantle would produce a fast polarization direction parallel to maximum extension (Fouch and Rondenay, 2006). Thus, it is important to recognize the underlying causes of anisotropy in order to understand the relationship between the localized stress field, observed anisotropy, and subsurface deformation.

LPO, the orienting of anisotropic minerals through deformation, is generally considered the dominant process producing anisotropy in the continental upper mantle (Silver, 1996). In order

to actually observe anisotropy from LPO, however, the minerals must not only be sensitive to the strain field so that the crystal lattices realign preferentially, but there must be also a large-scale process that generates coherent strain over a sufficiently large area in order to produce LPO that can be sampled on the length scale of a seismic wave (Silver, 1996; Montanger and Guillot, 2002). The exact relationship between LPO anisotropy and deformation is complex and dependent on the pressure, temperature, stress, volatile content, and melt fraction of the system. For example, partial melt may cause a transition in deformation style, modifying the formation of LPO. On the other hand, it may actually improve the efficiency of mineral orientation, increasing the effects of anisotropy on shear wave splitting (Savage, 1999). Thus it is crucial to understand the specific mechanisms of LPO formation to more precisely relate anisotropic observations to predictions of continental mantle flow (Long and Becker, 2010).

There are two different deformation processes that are prevalent at upper mantle conditions, with different consequences for LPO. Diffusion creep, as the name suggests, is deformation via diffusion between grain boundaries or across a crystal lattice. This deformation style is assumed to not produce preferred orientation and thus the mantle matrix remains isotropic (Savage, 1999). However, recent evidence suggests that diffusion creep can potentially produce LPO under certain conditions, namely, anhydrous, two-phase, low-stress systems (Sundberg and Cooper, 2008). Dislocation creep, in which deformation is accommodated via the movement of defects or irregularities within mineral grains, does produce LPO and thus anisotropy. In contrast to diffusion creep, dislocation creep occurs at high stress, low temperatures, and/or large grain sizes and produces a strain rate that increases nonlinearly with stress (Savage, 1999).

Olivine is the primary, though not the only, mineral responsible for LPO in the upper mantle. Other important anisotropic minerals may include: wadsleyite and ringwoodite in the transition zone; perovskite, post-perovskite and ferropericlase in the D” layer; and biotite and hornblende in the crust (Fouch and Rondenay, 2006; Long and Silver, 2009). However, in the mantle at depths of approximately 200-400km, olivine constitutes up to 40% of the content of typical mantle rocks such as peridotite. Because of structural differences between the three primary crystallographic axes of olivine, the mineral is highly anisotropic, depending on temperature, producing P-wave velocity variations of 6% to 13.9% (up to 25% according to some models) and

S-wave variations of 7.1% to 12%, in a single crystal (Nicolas and Christensen, 1987; Iturrino et al., 1991; Vinnik et al., 1994; Savage, 1999; Park and Levin, 2002). Only a modest alignment is necessary to produce anisotropies up to 2-6%, which is typical in much of the upper mantle (Park and Levin, 2002). Recent laboratory studies have discovered that the actual formation of LPO in olivine is far more complex than previously imagined and that there are at least five types of olivine fabric, distinguished from one another by their dominant slip mechanisms (Karato et al., 2008). While the actual fabric that develops is dependent on the conditions of deformation- including stress, temperature, volatile content, and pressure- the anisotropic fast direction is typically aligned with the direction of maximum shear for most fabric types, and thus generally parallel to flow direction. The one exception is B-type fabric, formed in relatively high-stress, low temperature conditions in the presence of water, in which the fast axes in the mineral tend to align orthogonal to maximum shear, and thus perpendicular to flow direction (Karato et al., 2008; Long and Becker, 2010).

2.2 Relating Anisotropy to Mantle Deformation and Tectonic Processes

Many of the complications associated with studying anisotropy in continental interiors center on the debate over whether anisotropy is due to tectonic deformation frozen in the lithosphere (and thus related to surface geological features) or convective asthenospheric flow (and thus related to the present-day absolute plate motion). Many studies, including those done in central Europe, have suggested that beneath the continents, the consistency of splitting observations with crustal strain supports the model of coherent lithospheric deformation; however, the debate remains unsettled (Savage, 1999).

Silver and Chan (1991) outline three candidate processes for producing the anisotropy observed globally beneath continents. The first is that anisotropy is the result of absolute plate motion, which would concentrate strain in the asthenosphere and produce fast polarizations parallel to asthenospheric flow and splitting parameters that vary smoothly across the plate. The second hypothesis is that anisotropy is strain-induced from lithosphere-wide stress, reflected in the present crustal strain field, due to processes such as basal drag from plate motion. The final model suggests that anisotropy is controlled predominantly by (past or present) tectonically

driven deformation in the lithosphere, so that fast polarizations are generally parallel to trends in surface structure or perpendicular to collision directions. The first model suggests that anisotropy is localized in the asthenosphere, while both the first and second models, as well as the third in tectonically active regions, predict that anisotropy is driven by contemporary processes. In stable continental interiors, the third model implies that anisotropy is due to fossil deformation in the lithosphere from past tectonic events (Silver and Chan, 1991).

Many studies on continental anisotropy have concluded that the primary cause of anisotropy is strain fossilized in the mantle following the last major episode of tectonic activity. A substantial piece of evidence for this conclusion is the significant association between fast splitting polarizations and the dominant direction of surface structural features in many continental settings (Silver and Chan, 1988). Similarly, the strong variability in anisotropy observed over relatively short lateral distances and across tectonic boundaries further supports the conclusion of another source of continental anisotropy beyond present-day mantle flow (Savage, 1999). Temperature is undoubtedly a crucial factor in fossilizing strain. Higher temperatures can enhance the process of mineral orientation, while a temperature below approximately 900°C is required to preserve the deformation over geologic time scales. Therefore, the cooling of the mantle following orogenesis and similar tectonic events is likely a critical step for recording fossilized anisotropic signature in the mantle (Silver, 1996; Savage, 1999). If in fact this third model proposed by Silver and Chan (1991) holds in Germany and similar continental settings, measurements of fossil anisotropy can be used to study the evolution and deformation history of continental plates (Silver and Chan, 1988).

There are of course local exceptions to this pattern, and the depth of observed anisotropy is a complicating factor for determining probable deformation scenarios. Anisotropy at shallow depths is indeed most likely due to older tectonic events in the subcrustal lithosphere, but deeper in the mantle, it may still be caused by recent deformations and present-day asthenospheric flow. Likewise, in some regions, localized flow patterns may help explain anisotropic parameters that are unrelated to surface features (Savage, 1999). In reality, anisotropy is most likely a result of a combination of lithospheric deformation and asthenospheric flow and determining a unique mode with certainty is nearly impossible with traditional methods.

2.3 Study Area and Tectonic Setting

The geological history of Germany has been dominated by three major tectonic events: The Hercynian orogeny in the center, the Alpine orogeny in the south and the Caledonian orogeny in the north (Bormann et al., 1993). Figure 2, taken from Winchester et al. (2002) displays the major crustal blocks and deformation belts in Germany.

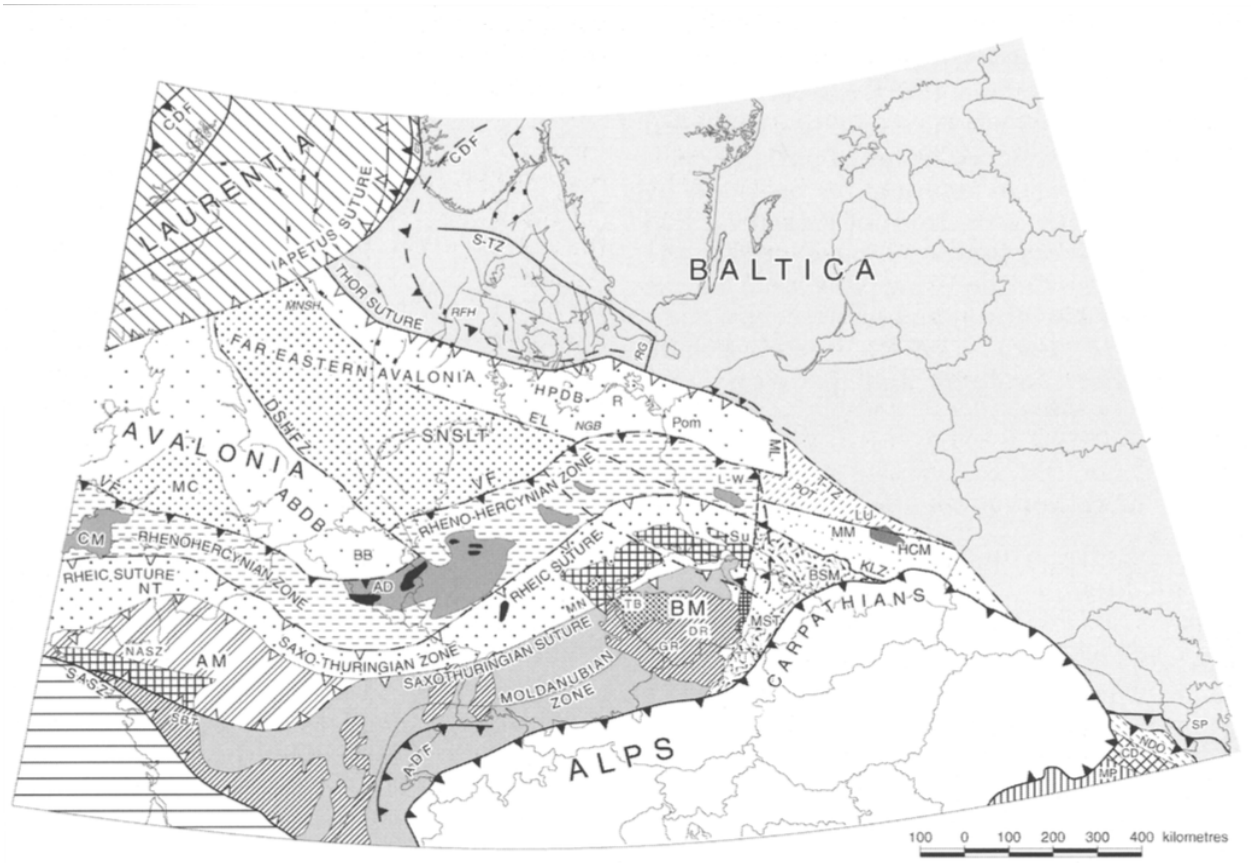

Fig. 2: Map showing the distribution of crustal blocks and deformation belts in Central Europe, taken from Winchester et al. (2002). Key to important abbreviations: ADF, Alpine Deformation Front; BM, Bohemian Massif; CDF, Caledonian Deformation Front; VF, Variscan Front

The Caledonian orogeny, referring to the collision of Laurentia, Baltica and Avalonia between 490-390 million years ago in the Early Devonian, caused the subsidence of a local continental rift zone, known as the Rhine Graben, and has shaped the western and northern border of the region. The Hercynian, or Variscan, orogeny was the Late Paleozoic collisional event between the Euramerica and Gondwana continents that formed the Pangaea supercontinent approximately

300 million years ago. This event is responsible for the typical NE-SW strike of the dominant geological surface features in western Germany (Zeis et al., 1990). Though specifically referring to the closure of the Rheic Ocean, the term Variscan is used more broadly to describe a longer deformational process from the mid-Devonian, at least 350 million years, up to the post-Stephanian age, less than 299 million years ago (Winchester et al., 2002). Lastly, the Alpine orogeny in the Late Mesozoic Era less than 100 million years ago refers to the collision of the African and Indian continents, and the smaller Cimmerian plate, with Eurasia, forming the Alps and causing uplift and faulting of the entire Variscan Unit (Zeis et al., 1990; Luschen et al., 1990). Figure 3, taken from Blundell et al. (1992) displays the approximate depth of the Moho across southern Germany, illustrating the rapid increase in crustal thickness under the Alps due to this orogenic event.

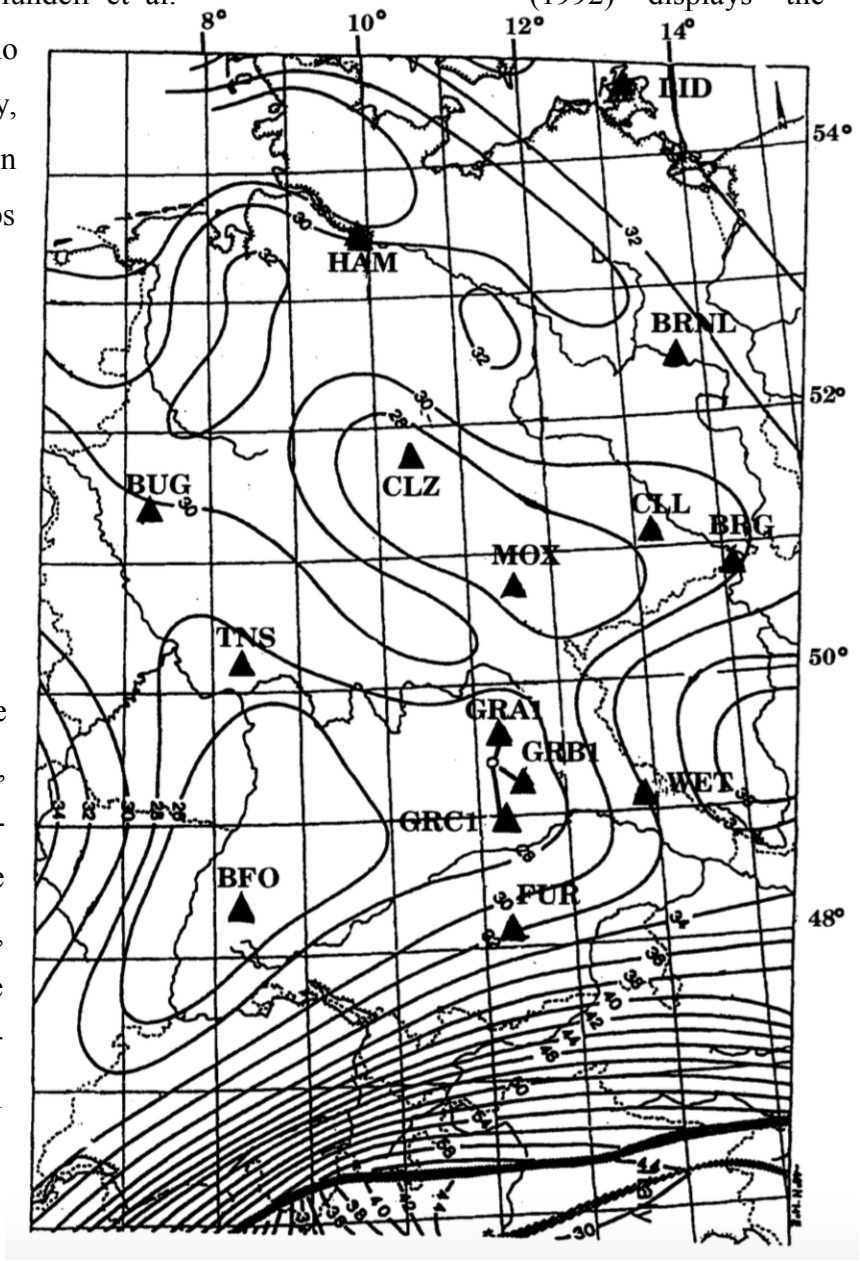

Fig. 3: Isolines of Moho depths in Central Europe and the locations of the German Regional Seismic Network Stations taken from Blundell et al. (1992)

To the east of the study area, the Trans-European suture zone, including the Tornquist-Teisseyre Zone, divides these western European mobile belts, such as the Variscan and Alpine units, from the 850 million year old East European Craton (Winchester et al., 2002).

The 'South-German Triangle' is a tectonic feature that dominates the southern portion of the study area. It is a structural sub-unit of the Hercynian, terminating in the west at the upper Rhine Graben and the Vogelsberg Mountains (trending NE-SW) and, in the east, at the Thuringian and Bavarian forests (trending NW-SE). The northern margin of the Alps is defined roughly as the unit's southern edge (Zeis et al., 1990). Most of the Triangle is covered by Mesozoic-age sediments, with a thickness that increases as one moves south up to 6km at the Alps. The western margin of the Triangle, in the Vogelsberg Mountains, is composed predominantly of volcanic rocks of late Tertiary age (Zeis et al., 1990). There remains a clear suture zone from the Variscan orogeny, which further divides the Triangle into the Saxothuringian zone in the north and the Moldanubian zone in the south (Zeis et al., 1990). Figure 4, taken from Bormann et al. (1993), illustrates the major tectonic elements of the South-German Triangle and the larger Hercynian unit.

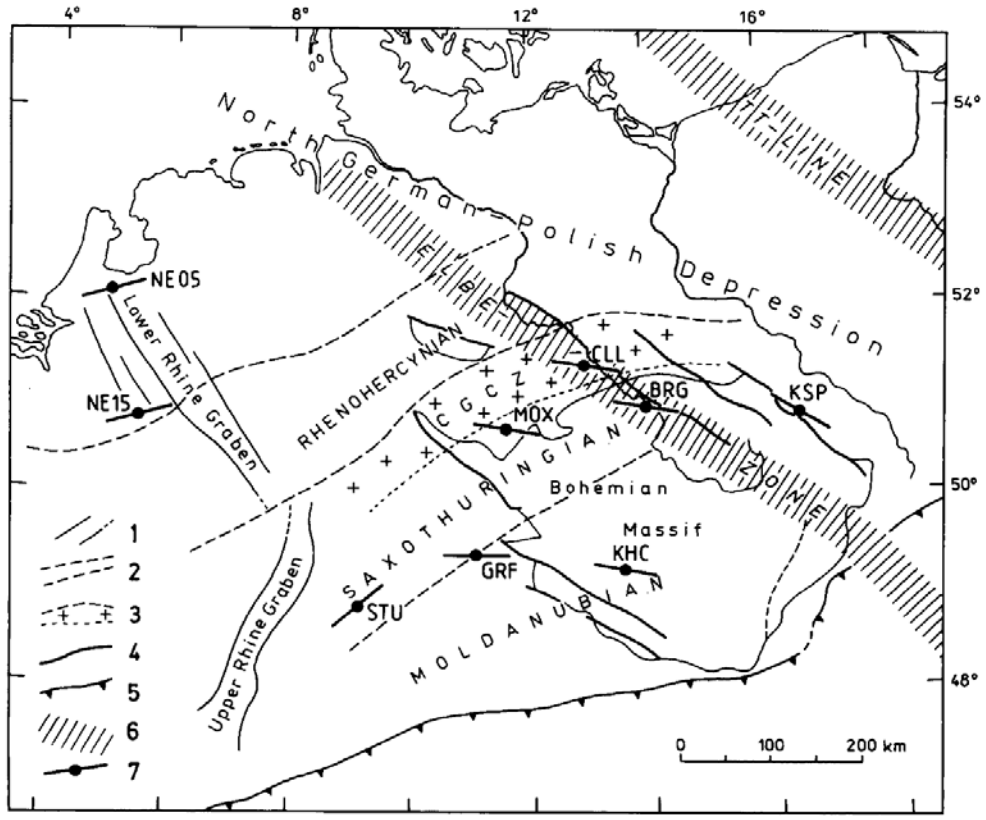

Fig 4: Major tectonic elements and zones of the Hercynian Unit in Central Europe taken from Bormann et al. (1993). Key to relevant symbols: 2, boundaries between the main fold belts of the Hercynian orogeny; 4, main faults with Hercynian (NW-SE) strike; 5, northern front of the Alps; 6, Tornquist-Teisseyre Zone; 7, positions of seismic stations and fast polarizations

The modern stress field of Germany has been shaped in part by all three of these major orogenic events and, as such, is highly complex, varying dramatically from east to west. The dominant trend of structural features transitions from NE-SW in the west to E-W in the middle and NW-SE as one moves east. These strikes are roughly orthogonal to the direction of maximum horizontal shortening in the crust, which is approximately N-NW in the west and N-NE in the east. Regional faults have observed strikes of 0-90° with respect to this direction of maximum shortening (Bormann et al., 1993). Grünthal and Stromeyer (1992) observed that the major forces shaping the crustal stress field were ridge push from the North Atlantic ridge and the relative motion of the African plate towards Eurasia. This general trend is modified locally by secondary effects and structural inhomogeneities due to differing elastic and rheological parameters within crustal blocks and changes in the depths of the Moho and lithosphere (Bormann et al., 1996).

2.4 Past Work on Anisotropy in this Region

A variety of studies have been done trying to characterize anisotropy beneath Germany, particularly in the south, though typically with different methods and less data than the present study; however, it is still useful to understand the results of this past work in order to validate and compare with our observations. Most of the past work done in this region indicates strong variations in the fast splitting direction with backazimuth and depth, implying that regional anisotropy is complex (Vinnik et al., 1994; Bormann et al., 1996). Through the analysis of head wave (Pn) velocity residuals, Bamford (1977) concluded that anisotropy was up to 7% to 8% in the mantle with a maximum P-wave velocity of 8.4km/s at a fast polarization of approximately 20° from north. Building off of this work, Enderle et al. (1996) found that anisotropy increased with depth up to 11% in an anisotropic structure 10km below the Moho, where P-wave velocities approached 8.03km/s in the fast direction and only 7.77km/s in the slow direction. This work found a similar average amount of anisotropy as Bamford (1977), but with a different distribution and a slightly different fast polarization of 31° clockwise from north. Wylegalla et al. (1988), also evaluating Pn residuals, estimated the amount of upper mantle anisotropy to be approximately 6% and found evidence of lateral variations in anisotropic parameters. However, in contrast to Bamford (1977) and Enderle et al. (1996), they observed what could be interpreted as two-layers of anisotropy, with fast directions at both 10° and 190°. Vinnik et al. (1994)

observed significantly different anisotropic patterns, with a fast SKS splitting direction which transitioned from 50-70° in the west to 100-120° in the east, in line with the approximate orientation of surface structural features.

Many of the studies done in this region, though utilizing different methods, have involved data from one or more of the stations used in this study and, as such, we can use these observations of anisotropic parameters at these stations for comparison. At station KHC, of the Czech Regional Seismic Network, Babuska et al. (1993) calculated a fast direction of 90° and a delay time of 0.6s. In contrast, Bormann et al. (1993) using P-wave refraction data, observed a delay time of 1.1s and a fast direction of 100° at this location. They also calculated that nearby station STU, from the Geofon Program Temporary Network, had a fast direction of 50° and a delay time of only 0.5s. Vinnik et al. (1992) had nearly identical results for station STU. The results found by Vinnik et al. (1994) at station TNS of the German Regional Seismic Network, located northwest of both KHC and STU, were intermediate with a fast direction of 80° and a delay time of 0.8s. Though this study utilized shear wave splitting of SKS phases, they had clear splitting data for only five events, clumped at backazimuths of approximately 45° and 255°. Using SKS splitting, Silver and Chan (1988) found a delay time of 0.85s and a fast direction of 79° at station GRF, which is located directly adjacent to GRA1 of the German Regional Seismic Network. These results diverged slightly from the fast direction of 88° and the delay time of 1.05s, observed by Silver and Chan (1991) directly for GRA1. This discrepancy is not surprising as there were only two well-observed SKS measurements for GRF and evidence suggests dramatic lateral variability in anisotropy over short length scales.

Some work has also been done with receiver functions for these stations in order to characterize crustal structure beneath Germany. Figure 5, reproduced from Zeis et al. (1990), shows a contour map of the approximate Moho depth in southern Germany. This map predicts a Moho depth of approximately 35km below station KHC, increasing southwards towards the Alps up to 39km under station DAVA, of the Austrian Broadband Seismic Network, and decreasing rapidly eastwards to only 27km under station STU. Blundell et al. (1992) corroborates these results, estimating a Moho depth of approximately 38km below DAVA, 36km below KHC, and closer to 26km under STU, as well as a depth of approximately 32km in the northeast near station RUE,

of the Geofon Program Temporary Network (Fig. 3). Kind et al. (1995) observed a similar pattern, with depths up to 32km near station GRA1 that become shallower towards the west, down to only 26km below station TNS. On a regional scale, Moho depths are quite consistent, ranging between 28km and 35km over much of Germany. The exceptions are a deep root, with Moho depths down to 60km under the Alps and the Tornquist-Teisseyre Zone, and a band of shallow crust in a SW-NE strike through the Rhine Graben (Enderle et al., 1996; Bormann et al., 1996). It should be noted that the previous receiver function analysis in this region has focused on characterizing isotropic structure, rather than anisotropy.

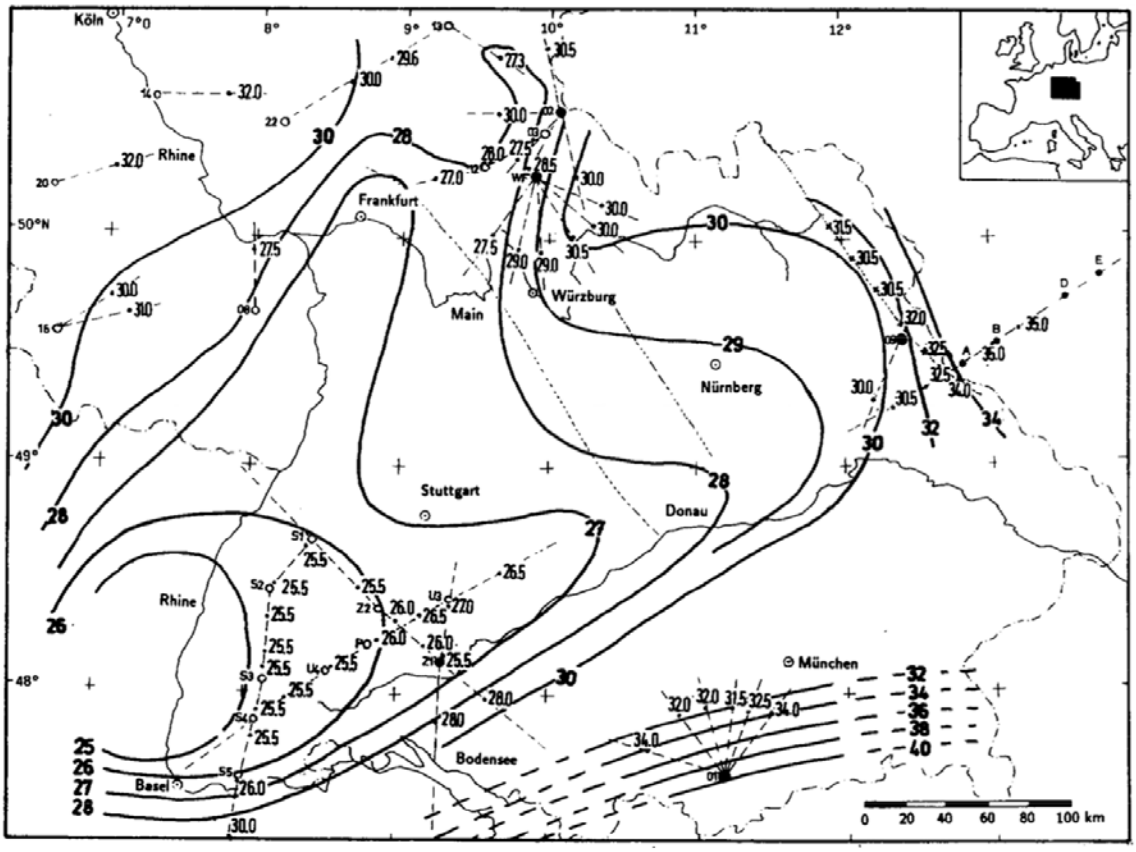

Fig. 5: Contour map of the Moho discontinuity in southern Germany with a contour interval of 1km, taken from Zeis et al. (1990)

As discussed in section 2.2, there are many possible interpretations for relating the observed anisotropy patterns to deformation models in the crust and mantle. In general, there seems to be a strong association in Germany between anisotropic parameters and structural features, implying that deformation frozen in the mantle from past tectonic events, particularly the Hercynian

orogeny, is a likely source of anisotropy (Silver and Chan, 1988; Bormann et al., 1993). Indeed, data from the regional strain field indicates a near-uniform NW-SE direction of plate motion across the region, which does not explain the transition in dominant anisotropic fast direction from NE-SW in the west to NW-SE in the east, and thus present-day asthenospheric flow cannot be the only source of anisotropy (Silver, 1996). Similarly, average splitting parameters from previous studies seem consistent across tectonic units, only changing near significant boundaries, such as the suture zone between the Saxothuringian and Moldanubian zone, and observed fast directions are typically parallel to the strike of the major deformation bands, like the Variscan Belt (Babuska et al., 1993; Bormann et al., 1993). Plenefisch and Bonjer (1994) also found an agreement between observed fast directions and fault plane solutions of crustal earthquakes in the western part of the region, though there is some discrepancy in the eastern and central part of Germany.

There is some disagreement with the finding that coherent deformation between the crust and lithosphere dominates the modern anisotropic signature. For example, Fuchs (1983) proposed a model in which the source of anisotropy is crustal stress reflected in the mantle down to at least 50km. In this model, the preferred orientation of olivine is almost perpendicular to the modern crustal stress field, and thus development of LPO-induced anisotropy is a recent process (Fuchs, 1983; Bormann et al., 1996). Similarly, Bormann et al. (1996) disagree with the fossil deformation model because of their inferred temperature in the mantle, which would make preserving anisotropy difficult. However, more recent studies, including that by Silver (1996) with improved data quality and resolution, suggest that the observed lateral and vertical heterogeneities in Germany are far too great and on too short a length scale for present-day flow to be the only cause of anisotropy. The disagreement in previous work reflects the impact utilizing particular techniques and stations can have on a study. It also illustrates the sort of simplifying assumptions made in this past work. This emphasizes the need for a more thorough analysis of structure beneath Germany that takes advantage of a variety of different techniques and accounts for possible complexity.

3 SHEAR WAVE SPLITTING: Methods, Results and Interpretation

3.1 Methodology

Shear wave splitting is a popular and practical technique for studying anisotropy, for a variety of reasons. The standard computational methods used in splitting analyses are relatively simple and straightforward, the use of phases such as SKS provides good lateral resolution, and, with adequate backazimuthal coverage, splitting studies can elucidate information about structural complexity (Fouch and Rondenay, 2006). Figure 6, reproduced from Long and Becker (2010), provides a schematic of the process of a shear wave splitting into orthogonally polarized fast and slow components with an associated delay time. The accumulated delay time depends on the strength of the anisotropic layer and the length of the path through that layer (Park and Levin, 2002; Fouch and Rondenay, 2006). The fast direction depends on the geometry of anisotropy. As with delay time, the polarization of the fast direction, φ, represents the path-integrated effects of anisotropy on the receiver side and is strongly dependent on the structure, size and geometry of the anisotropic layer (Fouch and Rondenay, 2006).

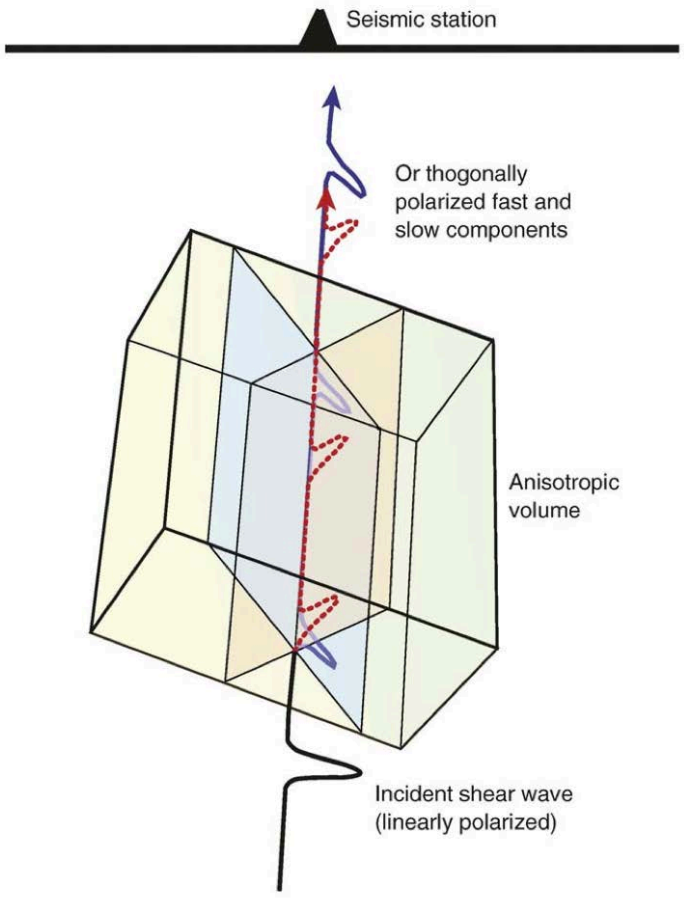

Fig. 6: Schematic of the process of shear wave splitting due to anisotropy, taken from Long and Becker (2010). The important parameters observed in this process are φ, which corresponds to the polarization of the fast component, and δt, which is the time delay between the fast and slow components.

Despite its benefits, it is recognized that the shear wave splitting approach has certain limitations. Acquiring data with robust backazimuthal coverage is difficult

in most places and it is estimated that a station must be recording for periods of many years for sufficient coverage in most regions. Furthermore, the phases typically used (such as SKS and SKKS) provide few vertical constraints on anisotropy (Fouch and Rondenay, 2006). On top of this, most splitting analysis methods assume one layer of anisotropy with a horizontal axis of symmetry, and require a good signal-to-noise ratio, and thus there can be significant uncertainty in studies in complex tectonic settings (Wüstfeld and Bokelmann, 2006). In these instances, it is possible to analyze the variation in splitting parameters with backazimuth in order to diagnose complex anisotropy, whether dipping or multi-layered (Fouch and Rondenay, 2006).

Despite its limitations, shear wave splitting has remained one of the most utilized methods for studying anisotropy, particularly since Vinnik et al. (1984) first investigated the splitting of the SKS phase. SKS and similar core phases, such as SKKS and PKS, have distinct advantages in regard to measuring anisotropy. The initial polarization of the shear wave is controlled by the P-to-S conversion at the CMB and therefore it is known; the polarization is assumed to be radial and thus corresponds to the backazimuth. The conversion from a P-wave also constrains the observed splitting to the subsurface on the receiver side of the path (Babuska et al., 1993; Wüstfeld et al., 2008; Long and Silver, 2009). SKS phases are best studied in the epicentral distance range of ~85° to ~120°, where the arrival will be distinct from the S and ScS phases, but also sufficiently energetic (Silver and Chan, 1988; Silver and Chan, 1991). Work on SKKS phases is focused on the distance range from ~90° to ~130° so that the wave will be isolated from the SKS arrival, while PKS phases are observed in the range from approximately 130° to 150° (e.g. Liu and Gao, 2013; Eakin et al., 2015). Because of their different arrival patterns, using a combination of these phases is particularly useful for increasing backazimuthal coverage. On top of this, at these epicentral distances, these waves have almost vertical incidence angles (<10° for SKS and <13° for PKS) and thus they can provide excellent lateral constraints on anisotropy (Eakin et al., 2015).

Often, *KS phases on a seismogram arrive with no sign of having been split, in what is called a null measurement. This may occur when there is no anisotropy along the wave's path. However, it may also indicate that the initial polarization of the shear wave is parallel to the fast or slow direction of the anisotropic structure, and thus null measurements can be useful for constraining

the geometry of the medium (Park and Levin, 2002; Long and Silver, 2009). Similarly, at some stations, null measurements are observed over a wide swath of backazimuths. This can be evidence of isotropy or very weak anisotropy. It can also be interpreted as destructive interference between different anisotropic layers in the same medium or an anisotropic layer with a vertical axis of symmetry (Park and Levin, 2002). Recognizing the extent and causes of null *KS arrivals is thus a crucial component of diagnosing more complex anisotropic structure.

The most widely used method for characterizing anisotropy from shear wave splitting is the transverse component minimization method, proposed by Silver and Chan (1991) and henceforth referred to as the SC method. This technique is based on the principle that, due to the conversion at the CMB, an *KS wave is radially polarized in the plane containing the source and receiver and, therefore, there should be no energy on the transverse component (Silver and Chan, 1988; Liu and Gao, 2013). Consequently, detection of transverse energy on a seismogram, manifested in elliptical particle motion, is a clear indicator of a deviation from the isotropic scenario, suggesting the presence of anisotropy (Silver and Chan, 1991; Long and Silver, 2009). The SC method utilizes a grid approach to identify the splitting parameters (fast polarization and delay time) that minimizes the magnitude of transverse-component energy (and consequently linearizes particle motion), in order to account for the effect of splitting (Silver and Chan, 1988; Long and Silver, 2009). Formal errors in this method are estimated using a statistical F-test for a value of significance, α, equal to 0.05 (Silver and Chan, 1988; Silver and Chan, 1991).

Another popular computational technique is the cross- or rotation-correlation method, known henceforth as the RC method, which, despite certain advantages, is often considered more useful as a reference measurement relative to the results obtained via the SC technique. The RC method is based on the principle that splitting due to anisotropy will produce two orthogonally polarized components with identical pulse shapes. Like the SC method, RC employs a grid search to identify the best-fitting splitting parameters that maximize the correlation between these two pulses when they are rotated and time-shifted to overlap (Long and Silver, 2009). Generally, it is accepted that the SC method is the more robust technique when handling noisy data (Long and Silver, 2009). Similarly, transverse energy minimization typically provides a wider backazimuthal range of good measurements and more robust estimates of fast polarization near

null directions (Wüstfeld et al., 2008). However, the appeal of rotation-correlation is that the results obtained from the two methods can be compared in order to identify the true null direction, at which point the difference in fast direction should be an integer multiple of 45° (Wüstfeld and Bokelmann, 2006).

3.2 Data and Methods

In this study, we analyzed the splitting of SKS, SKKS and PKS arrivals for events with a magnitude range of 5.8 and greater, over the epicentral distance range 88°-150°. For those events for which we detected multiple arrivals, the splitting parameters observed for each waveform were compared and discrepancies were noted. Such differences in observed parameters for SKS and SKKS phases is a possible indicator of a contribution to anisotropy from the D" layer (e.g. Long and Silver, 2009). Arrivals were analyzed on three-component seismograms from ten broadband stations in and around Germany. Table 1 lists the stations used in this study. Nine of these stations were available in the archives of the IRIS Data Management Center and all available data was acquired. For station TNS, of the German Regional Seismic Network, data was collected through the BRG Orfeus Center. Due to difficulties with their request system, fewer events were available at this station, despite the relatively long time record. However, every station had multiple years of data available, translating into at least 400 candidate events per station, and relatively good backazimuthal coverage. A 6° clockwise realignment had to be applied to RUE to adjust for an obvious mis-orientation, based on observed SKS polarizations.

The shear wave splitting analysis was performed with the Splitlab software package (Wüstfeld et al., 2008). For all events, a bandpass filter, typically 0.01-0.1Hz was applied in order to maximize the signal-to-noise ratio. The precise cutoff frequencies were adjusted for individual events. The low frequency boundary varied from 0.01-0.02Hz, while the high frequency varied from 0.083-0.125Hz. The best-fit splitting parameters were logged for every waveform for which we obtained a well-constrained measurement. Null arrivals were also recorded for those events that displayed a linear uncorrected particle motion, a visible pulse on the radial component, and no energy above the noise on the transverse component. Both splits and nulls were then classified as poor, fair or good. The 'poor null' classification was reserved for those

measurements that displayed some energy on the transverse component, but not enough to obtain a well-constrained measurement. However these 'near nulls' were not included in any subsequent data analysis or plotting. Some previous splitting studies have employed a stacking method to help compensate for noisy data and poor waveform clarity. However, these techniques assume that anisotropy is single-layered and homogenous and thus lose valuable information about potential heterogeneity (Long and Silver, 2009). For this reason, no stacking method was used in this study.

Network	**Station Code**	**Latitude, Longitude**	**Available Data**
Czech Regional Seismic Network (CZ)	KHC	49.13, 13.58	1976-1985, 2003-2012
Danish National Seismic Network (DK)	BSD	55.11, 14.91	2009-2012
Danish National Seismic Network (DK)	MUD	56.46, 9.17	2009-2013
Austrian Broadband Seismic Network (OE)	DAVA	47.29, 9.88	2009-2013
Geofon Temporary Network (GE)	STU	48.77, 9.20	1994-2006
Geofon Temporary Network (GE)	WLF	49.66, 6.15	2000-2006
Geofon Temporary Network (GE)	RUE	52.48, 13.78	2000-2006
Geofon Temporary Network (GE)	IBBN	52.31, 7.77	2001-2006
German Regional Seismic Network	GRA1	49.69, 11.22	1990-2002
German Regional Seismic Network	TNS	50.22, 8.45	1991-2014

Table 1: Network, station code, location, and length of data recording for the ten stations used in this shear wave splitting analysis

SplitLab calculates best-fit splitting parameters (fast direction and delay time) using both the SC (transverse energy minimization) and RC (rotation correlation) methods. Because of its advantages, discussed in section 3.1, we henceforth only present results obtained with the SC method. However, we only retained data for events that yielded relatively similar results for both methods. Wüstfeld and Bokelmann (2007) recommend keeping only those splitting events where the difference in fast direction calculated by each method is less than 22.5° and the ratio of the calculated delay times ($\delta t_{RC}/\delta t_{SC}$) is greater than 0.7. They also suggest characterizing a splitting measurement as 'good' only if the ratio of delay times is between 0.8 and 1.1 and the difference in fast direction is less than 8°. A 'good' null measurement is defined as one with a small ratio of delay times, less than 0.2, and a difference in fast direction between 37° and 53°. We relaxed these criteria slightly, given how noisy the data was, but we did use them as guidelines when visually inspecting individual seismograms. Qualitative quality-assurance indicators for split measurements, adopted from Park and Levin (2002), included similarity in shape of the fast and slow component arrivals and, following the corrections to compensate for splitting, a minimal amount of energy on the transverse component and the linearization of the original elliptical particle motion.

3.3 Splitting Results

For all ten stations of this study we observed a combination of split and null observations, as well as many 'near null' measurements that displayed some characteristics of both. The majority of splits were classified as poor or fair. Figure 7 provides an example of both a good split and a good null SKS-phase measurement. The good null was recorded at station GRA1 from a magnitude-7.0 event in May 1995 while the good split was recorded at station KHC from a magnitude-6.4 event in November 1979.

Fig. 7 (next page): Examples of a good null (top) and good split (bottom) measurement at stations GRA1 and KHC, respectively. Key to panels: Top left, the radial (dashed blue line) and transverse (solid red line) components of the original seismogram with the increment used in splitting analysis highlighted in gray; Middle row, diagnostics for the rotation-correlation method; Bottom row, diagnostics for the transverse component energy minimization method; Left, corrected fast (dashed blue line) and slow (solid red line) components; Center left, the corrected radial (dashed blue line) and transverse (solid red line) components; Center right, the initial particle motion (dashed blue line) and the corrected particle motion (solid red line) without the effects of splitting; Right, contour plot of the correlation coefficient with the best-fitting splitting parameters shown with the crossed lines and the 95% confidence region indicated in gray.

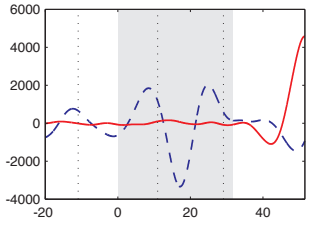

Event: **05-May-1995 (125) 03:53 12.62N 125.31E 33km Mw=7.0**
Station: **GRA1** Backazimuth: **63.5″** Distance: **95.23″**
init.Pol.: **245.9″** Filter: **0.010Hz - 0.10Hz** SNR_{SC}:**28.5**

Rotation Correlation: 87< -71° < -48 0.0<0.2s<0.4
Minimum Energy: 64< -63° < -31 0.1<0.2s<3.7
Eigenvalue: -31< -27° < -29 1.5<3.7s<4.0
Quality: **good** IsNull: **Yes** Phase: **SKS**

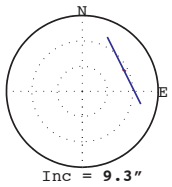

Table 2 contains the average best-fit splitting parameters,

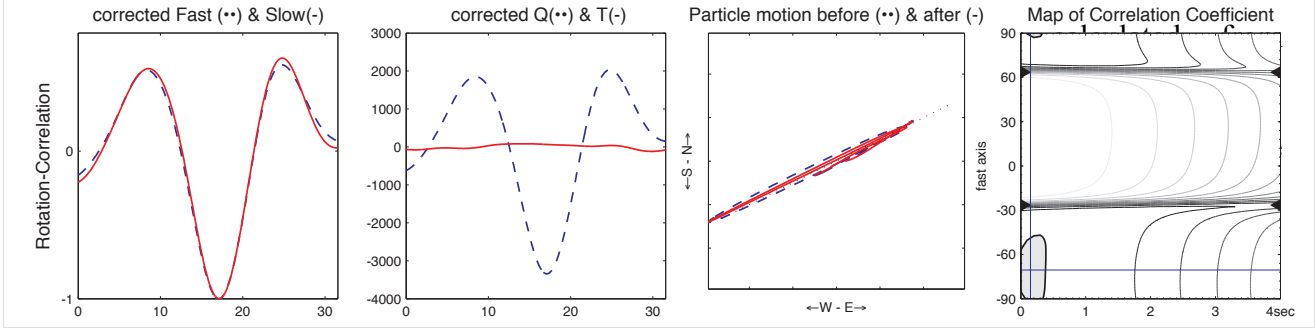

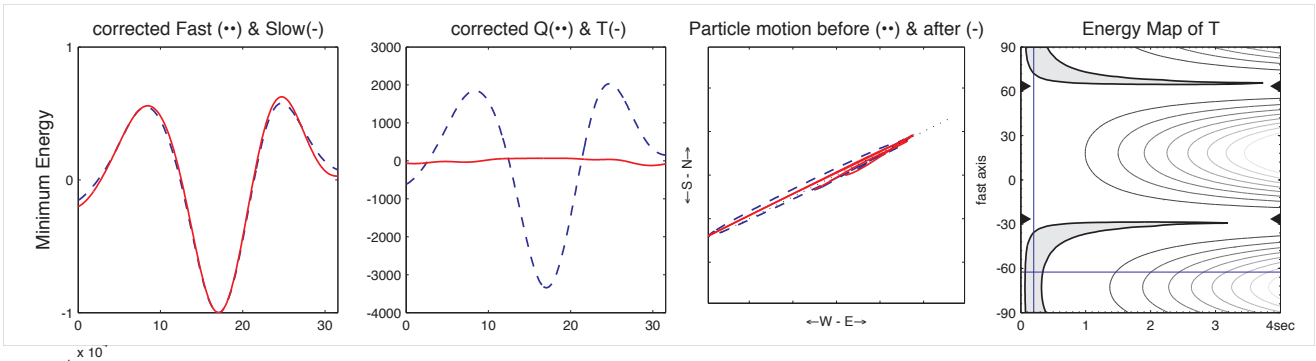

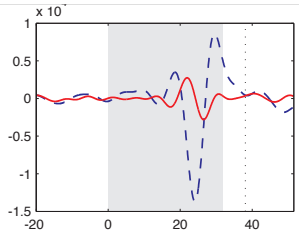

Event: **22-Nov-1979 (326) 02:41 -24.34N -67.39E 169km Mw=6.4**
Station: **KHC** Backazimuth: **247.2″** Distance: **102.60″**
init.Pol.: **69.9″** Filter: **0.020Hz - 0.12Hz** SNR_{SC}:**27.4**

Rotation Correlation: -75< -54° < -40 0.7<0.9s<1.2
Minimum Energy: -86< -77° < -68 0.8<0.9s<1.1
Eigenvalue: -68< -55° < -48 0.8<0.9s<1.1
Quality: **good** IsNull: **No** Phase: **SKS**

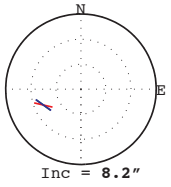

backazimuth of the splitting results for each

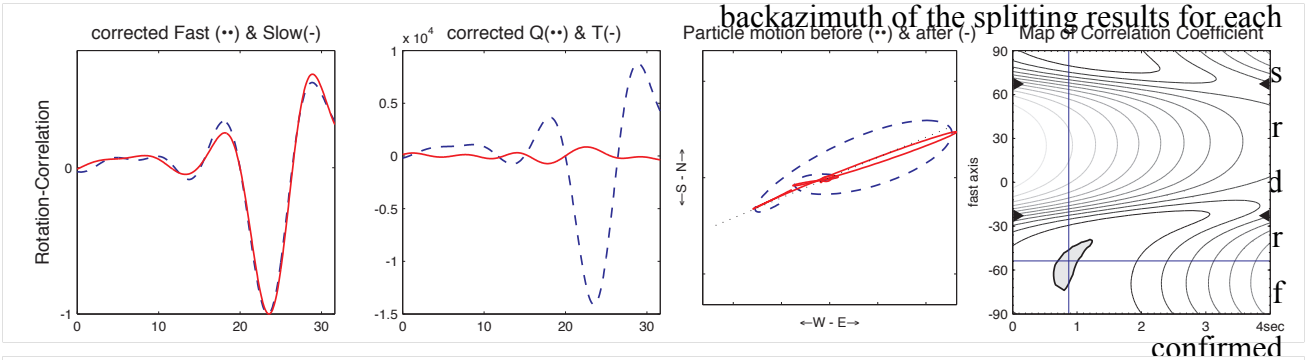

s
r
d
r
f

confirmed

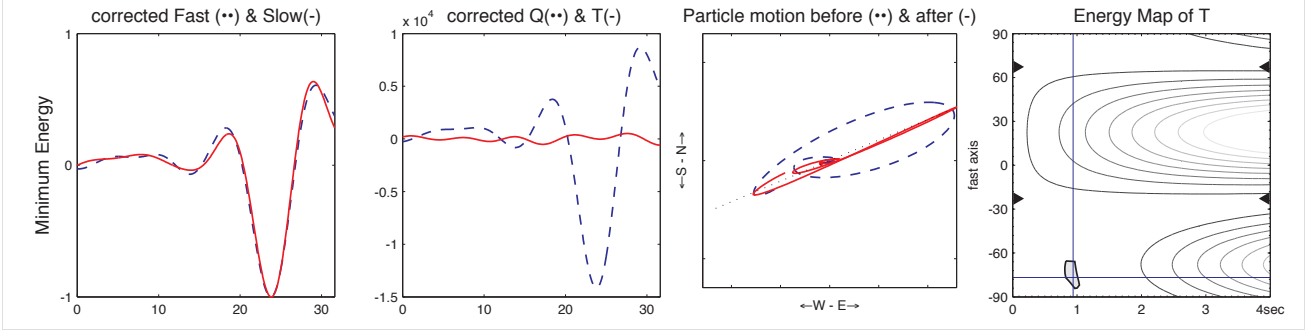

Table 2 contains the average best-fit splitting parameters, calculated from the SC method, and the average backazimuth of the splitting results for each station, as well as the total number of results and the number of confirmed splitting measurements. While it is possible for small delay times to obscure weak anisotropy, the relatively large average delay time recorded at every station increases our confidence that we are not mistakenly classifying splits as nulls because of small delay times due to weak anisotropy.

Station	# Results	# Splitting Measurements	Backazimuth (° from North)	Fast Direction	Delay time (seconds)
KHC	251	33	44.79, 248.25	-88, -71	1.3, 1.2
MUD	34	3	260.22, 15.64	-68, 40	0.7, 1.3
BSD	64	7	255.44	33	0.8
STU	83	10	41.48, 85.75	85, 32	1.9, 1.4
IBBN	44	4	266.12	-36	1.5
DAVA	50	10	82.01, 290.04, 198.53	40, 58, 53	1.3, 1.6, 1.7
RUE	134	10	248.51, 56.94	90, -76	1.0, 1.2
WLF	123	15	41.00, 242.54	83, -67	1.4, 1.0
GRA1	143	16	248.14	83	2.3
TNS	88	8	42.00	63	1.6

Table 2: Number of results, number of confirmed splitting measurements and then backazimuths and average best-fit splitting parameters for every station in the study. For those stations with two or three values in a column, we observed multiple distinct groupings of split measurements and thus each value represents the average parameter of each grouping. The order of the values is consistent between columns.

Figure 8 displays the average splitting parameters for each station in map view. Triangles represent the stations while the lines illustrate the orientation of the fast direction and average delay time recorded at each station. For those stations with distinct groups of split measurements at multiple backazimuths, there is an individual line to represent each group to illustrate variations in splitting parameters by backazimuth.

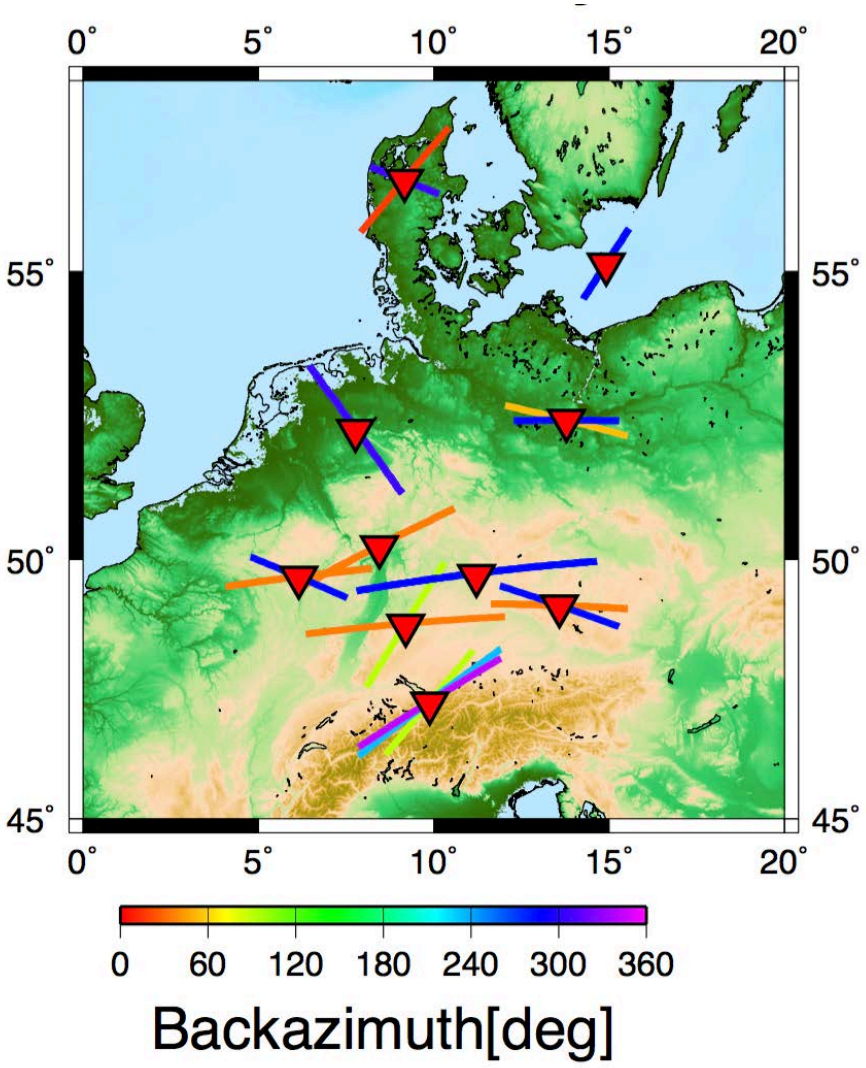

Fig. 8: Plot of average splitting parameters at individual stations. The orientation of lines represents the approximate fast direction at that station while the length of the line displays relative delay time. For those stations where there are multiple lines, each one (colored by backazimuth) illustrates the average splitting parameters at a different bacakzimuthal swath.

The quality assurance guidelines used for comparing the results from the RC and SC methods, discussed in section 3.2, meant that we only had a few 'good' quality splits, as we often observed a disagreement between the two methods for our splitting measurements, particularly in terms of delay time. Because of the subjectivity inherent in our classification system, we visually inspected all of the data repeatedly, especially to avoid changing standards when classifying data between stations and at the same station over time. However, according to Long and van der Hilst (2005), the two methods are likely to disagree at a station with more complex splitting parameters and thus the discrepancies we observed were not entirely surprising. Other potential issues we had to account for in our data that may have influenced our results included: distinguishing noise from signal, non-*KS arrivals in the window of analysis, and mis-orineted or faulty sensors (Liu and Gao, 2013).

For those stations where measurements of nulls and splits overlapped at the same backazimuth, results were again inspected to confirm their classification and identify any patterns in the overlaps. All of the overlapping measurements were confirmed and no clear pattern was identified. At some stations, including DAVA and GRA1, the overlapping nulls tended to occur earlier in time than the splits while, at station STU, the nulls occurred later in time than the splits. However, we observed no significant systematic relationships that would suggest that splitting patterns were changing in time.

We also kept track of those events for which we had measurements for both SKS and SKKS arrivals to determine if there were any discrepancies in these event pairs. Almost all of these pairs involved null arrivals for both phases. At station TNS there was one event, at a backazimuth of 42°, where the SKS and SKKS arrival were both classified as poor splits. However, the difference in fast direction was only 8°, which, given that the data was quite noisy, is well within the margin of error. There were no events where one phase produced a split measurement and the other a null, limiting our ability to constrain anisotropic patterns in the D" layer.

Figure 9 illustrates the results for each station individually with stereoplots. In these stereoplots, null measurements are represented as red triangles, while splits are plotted as lines oriented in the fast direction and scaled by delay time. The location where measurements are plotted is determined by the incidence angle (distance from the center of the circle) and backazimuth (with due North defined as 0°). We created three plots for each station. The first, not shown here, incorporated all results, including near nulls. The second, called the 'fair' plot includes all splitting measurements and only those nulls classified as fair or good. The final, 'good' plot includes only good nulls and only fair or good splits. We have included both the good and fair plots in order to display only those results we are most confident about without losing valuable information on possible backazimuthal variations in splitting.

Fig. 9: Stereoplots illustrating all results for individual stations. On the left (red and black) are the 'fair' stereoplots (all splitting measurements, only good and fair nulls) while on the right (blue and red) are the 'good' stereoplots (only fair and good splits, only good nulls). Measurements are located at the incidence angle (distance from center of circle) and backazimuth (location in circle) of the event. Triangles represent null measurements and lines represent splits, with the orientation and length of the line corresponding to fast direction and delay time, respectively.

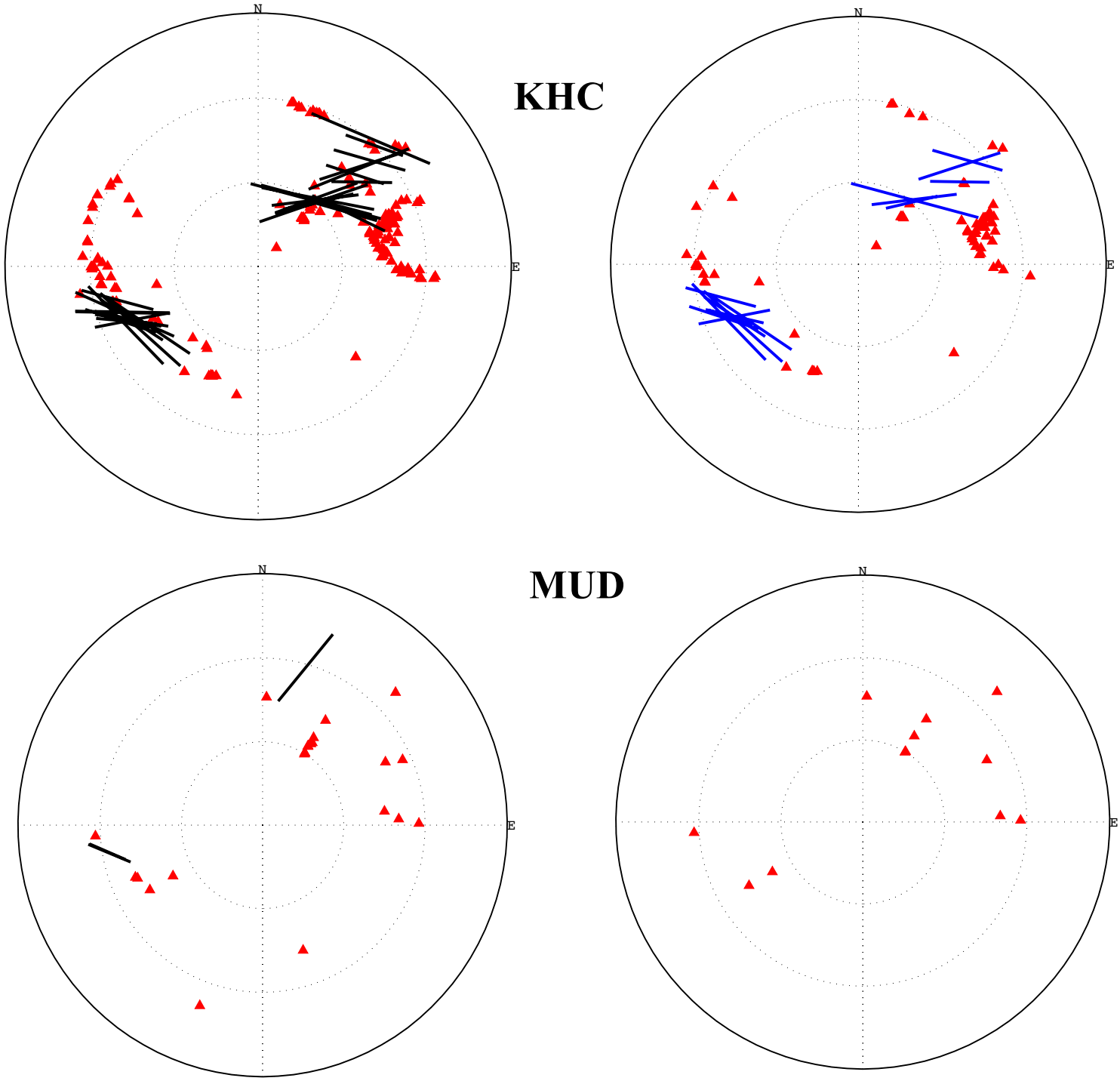

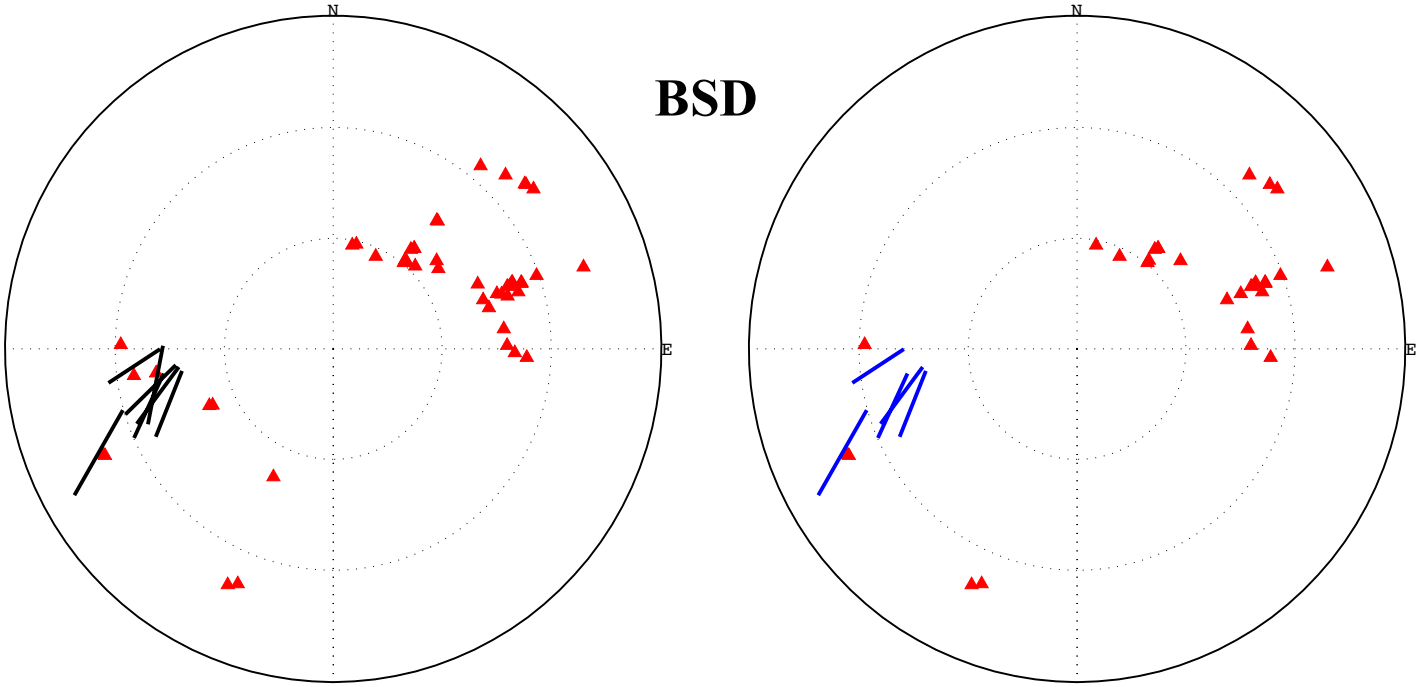
BSD
N
E
N
E

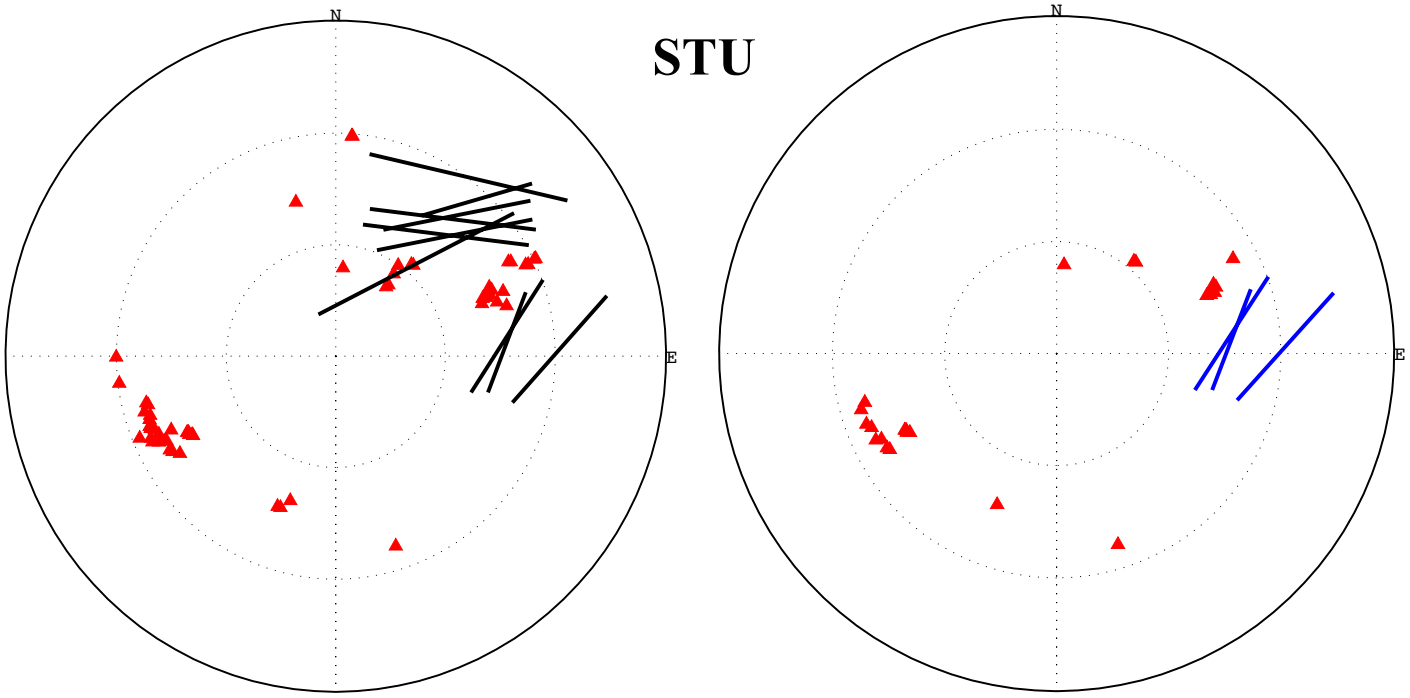
STU
N
E
N
E

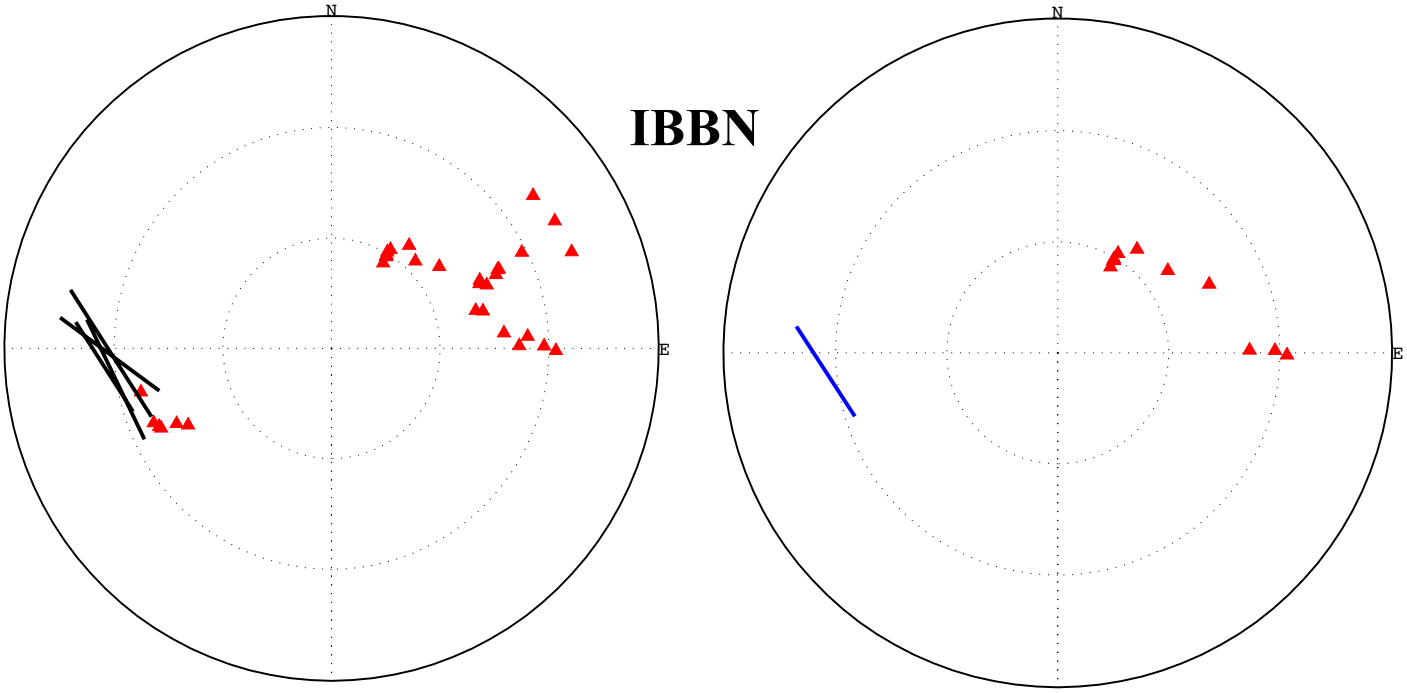
IBBN
N
E
N
E

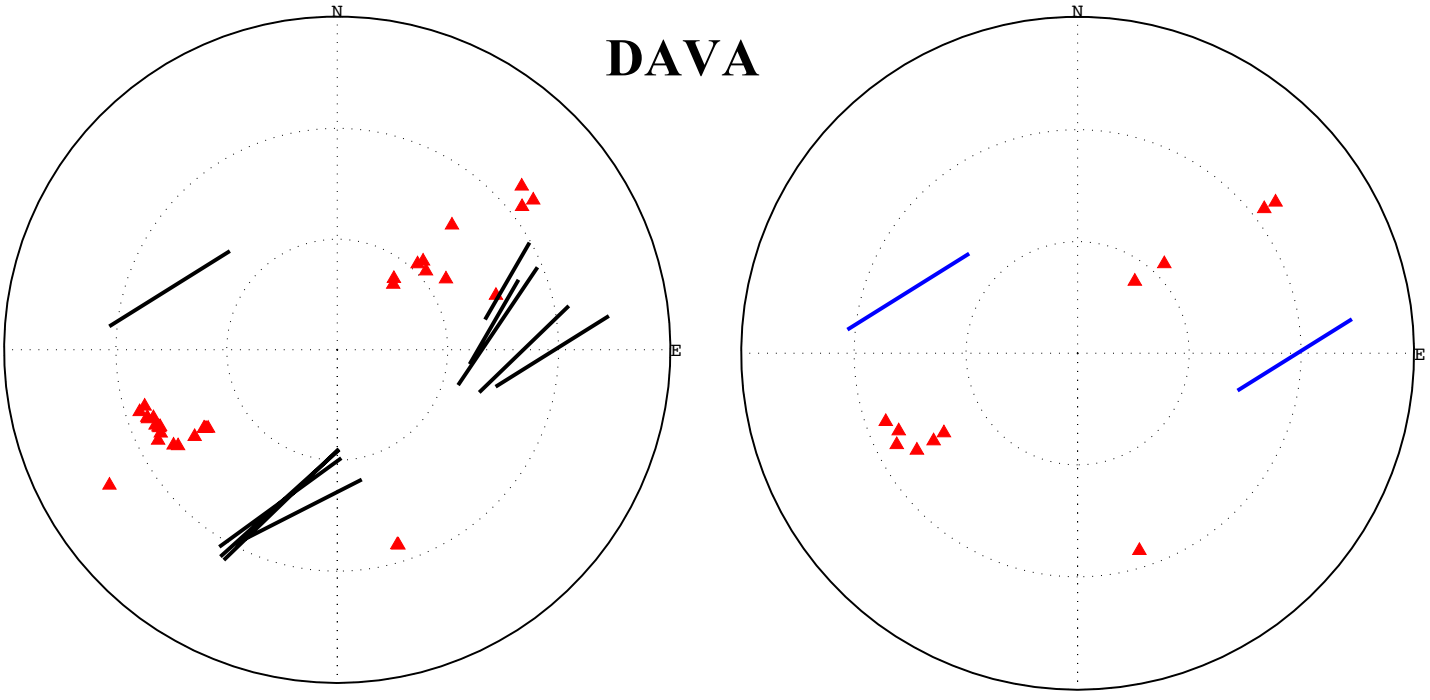
DAVA
N
E
N
E

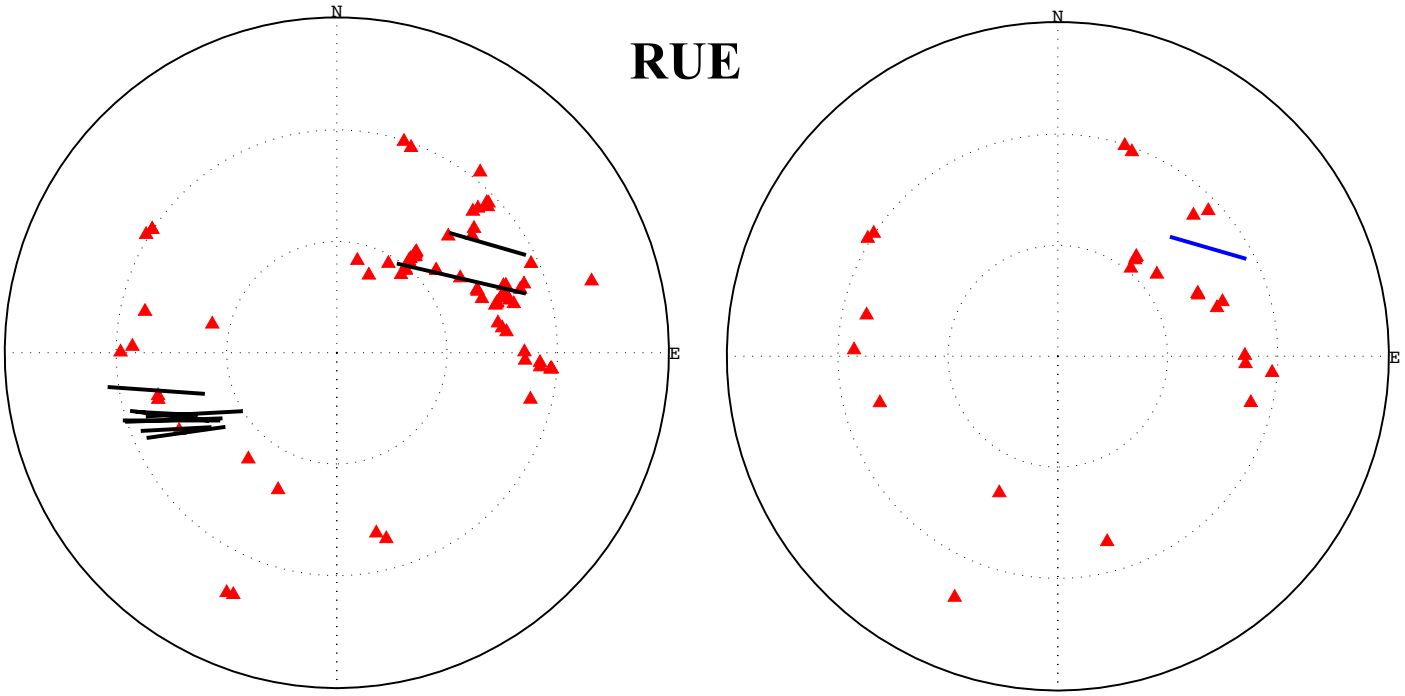
RUE
N
E
N
E

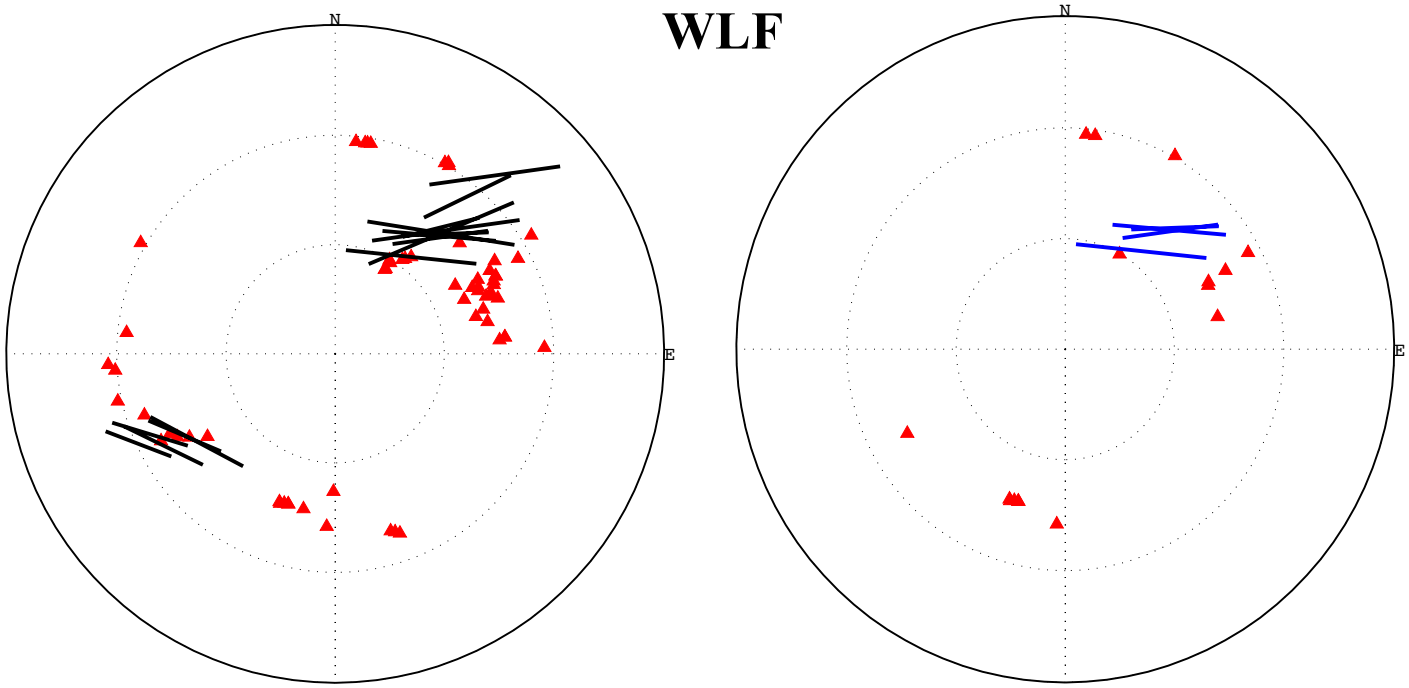
WLF
N
E
N
E

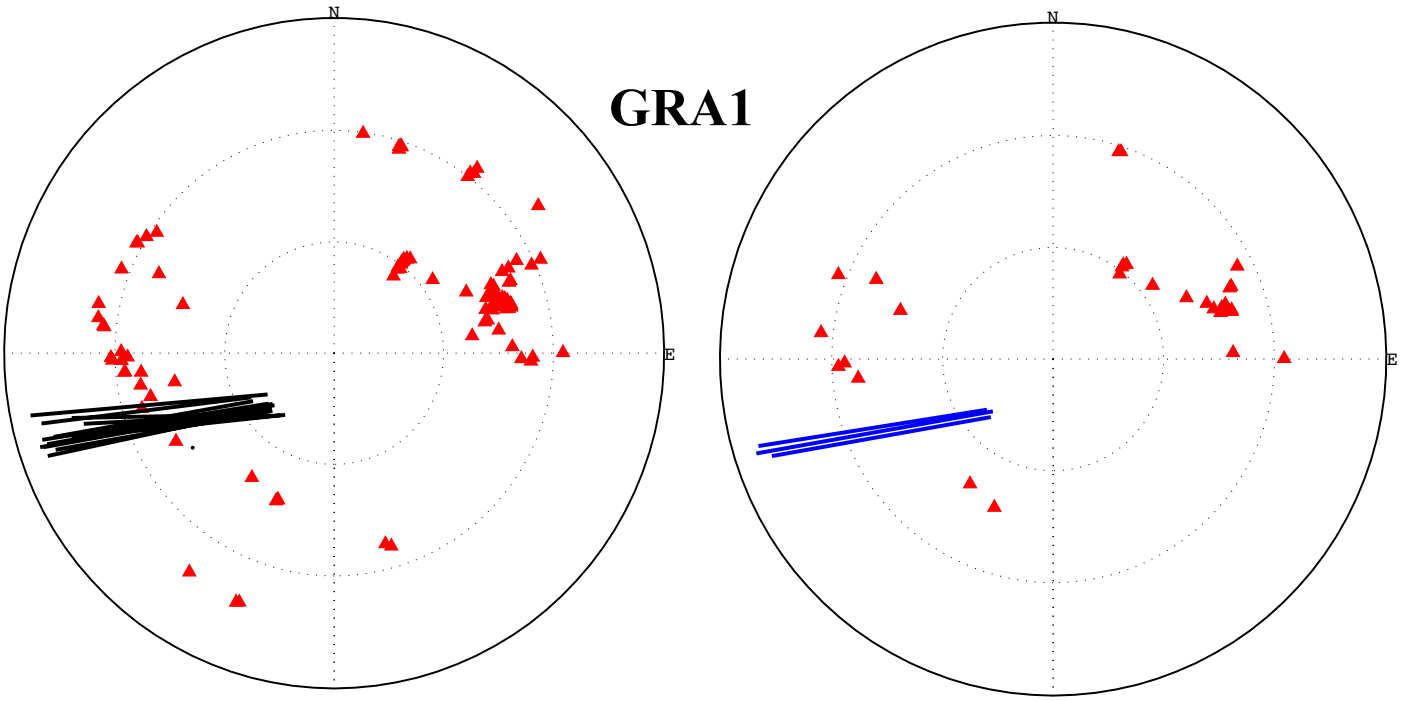
GRA1
N
E
N
E

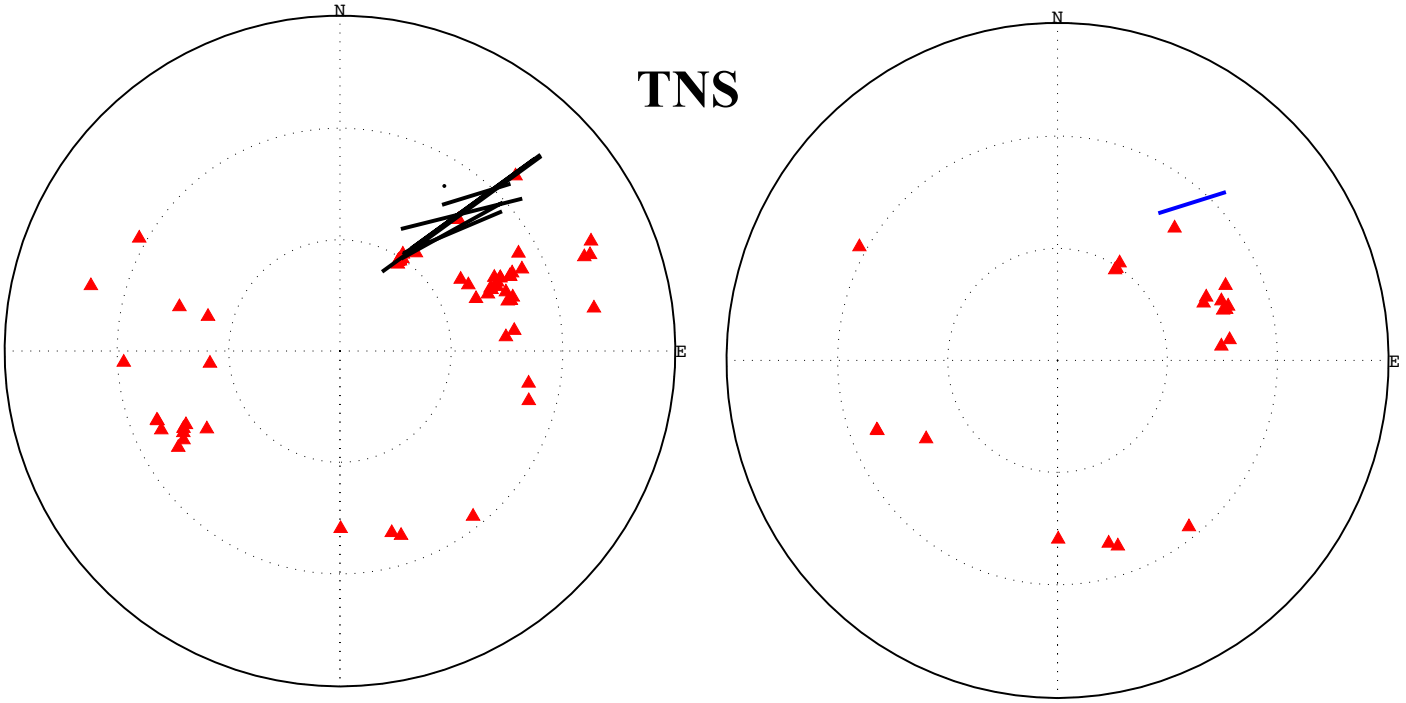
TNS
N
E
N
E

3.4 Interpretation

One of the main goals of this study was to see how our results compared to past work on anisotropy in this region. At station KHC, Babuska et al. (1993) observed a fast direction of 90° and a delay time of 0.6s, while Bormann et al. (1993) calculated a delay time of 1.1s and a fast direction of 100°. Unlike these studies, we observed two distinct groups of splitting measurements with similar splitting parameters of -88° and -71° with delay times of 1.3 and 1.2s, respectively, closer to those of Bormann et al. (1993). There is a similar pattern at station STU. Here, Vinnik et al. (1992) and Bormann et al. (1993) recorded a simple anisotropic structure, with a fast direction of 50° and a delay time of 0.5s, while we observed a more complex pattern with two backazimuthal groups with splitting parameters of 85° and 1.9s and 32° and 1.4s. While the average fast direction is relatively similar, there is a clear pattern where we observed much longer delay times, quite dramatically so, than previous studies. At GRA1, our station with some of our best splitting results, we observed a fast direction of 83° and a delay time of 2.3s compared to 88° and only 1.05s calculated by Silver and Chan (1991). While this station displayed clear evidence of splitting, our dataset is characterized by admittedly large discrepancies between the delay times calculated by SC versus the RC method with the former often estimating unusually high delay times. At station TNS we observed a fast direction of 63° and a delay time of 1.6s versus 80° and 0.8s according to Vinnik et al. (1992). That study located splitting events at backazimuths around 45° and 250°, which is a similar backazimuth observed for most of our stations.

More generally, Bamford (1977) and Enderle et al. (1996) found simple one-layered anisotropy with a fast direction of roughly 20° and 31°, respectively, averaged across the region. In contrast, Vinnik et al. (1994) found laterally heterogeneous anisotropy where the fast direction varied from 50-70° in the west to 100-120° in the east. Bormann et al. (1996) also observed a transition in fast directions from 40-50° in the west to approximately 90° in the center and 110-120° in the east. The pattern observed in this study was far more along the lines of that of Vinnik et al. (1994) and Bormann et al. (1996), with splitting parameters that varied between individual stations and across the region as a whole. Nevertheless, while we did see a rough transition in fast direction from predominantly NE-SW in the west, with fast directions between roughly 30-

80°, to E-W/NW-SE in the center and further east, with typical fast directions between 80-120°, our results were far more complex than this simple pattern. At the stations we defined loosely as 'in the west,' including WLF, TNS, STU, DAVA, IBBN and MUD, we also observed fast directions like 113° at WLF and 112° at MUD at different backazimuthal ranges. IBBN, up in the northwest, diverged most dramatically from this pattern, with a fast direction of -36 (144)°. Likewise, we observed a fast direction of only 33° at BSD, one of the more eastern stations. Unfortunately there has not been as much work done in northern Germany and so we cannot compare our results for BSD, MUD, and IBBN more directly to past work.

Our results for *KS splitting can be loosely categorized into three groups, each with a different characteristic splitting pattern. DAVA is a group unto itself as it is the only station that displays the relatively straightforward pattern of single-layered anisotropy. There are three groups of splitting measurements at different backazimuths, each displaying similar splitting parameters of approximately 50° fast direction and 1.5s delay time. On top of this, the majority of the null measurements are observed at backazimuths parallel and perpendicular to the splits as is expected for one layer of anisotropy. The next grouping (stations KHC, WLF, and RUE) can loosely be defined as those that display characteristics similar to what one would expect for multiple layers of interfering anisotropy. There are generally two groups of splitting measurements, focused at backazimuths around 45° and 250°, that display dramatically different characteristic splitting parameters. At KHC, the resulting parameters are quite similar between the two backazimuthal groups; however, what distinguishes this station from DAVA and places it into this second category is the preponderance of nulls at all backazimuths. The final category (stations TNS, IBBN, BSD and GRA1) reflects no obvious pattern and clearly displays complex anisotropy and lateral heterogeneity. At these stations there is only one group of split measurements at typical backazimuths of around 40° or 250°. There are also null measurements over wide swaths of backazimuths. STU and MUD display characteristics of both the second and third category and are both clear evidence of complex anisotropy. At both stations there are nulls at a wide swath of backazimuths and two groups of splits displaying no coherent pattern in splitting parameters or backazimuth.

Figure 4 emphasized that splitting parameters vary dramatically by backazimuth at almost all stations. However, there does seem to be a pattern where fast directions reflect the dominant

trends of surface features, particularly the Variscan deformation belts, from roughly NE-SW in the west to slightly E-W in the middle, towards NW-SE in the east. However, none of the results for these stations can be interpreted so simply. In fact, for events from a backazimuth of 50°, there appears to be a consistent trend observed throughout the region across tectonic boundaries, while there is more obvious heterogeneity within and between structural units from events at others backazimuths.

At KHC, in the central-east part of the region and in the Moldanubian unit, we predicted a transition to a NW-SE strike fast direction compared to STU, which is farther to the east and in the Saxothuringian unit. Despite the different tectonic structure, both stations, for a backazimuth of around 50°, display a consistent, almost E-W, trend in fast direction, though not in delay time. However, STU is also sampling events from a backazimuth closer to 150°, for which the NE-SW trend, which also reflects the strike of the Upper Rhine Graben farther east, is very visible. Similarly, for events arriving at KHC from a backazimuth of around 250°, there is a transition towards the NW-SE trend, which corresponds to the strike of a major Hercynian-age fault zone right near that station. GRA1, which is the in the same unit as STU, but closer to KHC, reflects the same almost E-W trend in fast direction, but with a much longer delay time and for events with a backazimuth of 250°. It should be noted that the fast direction displayed at GRA1 almost perfectly parallels the nearby tectonic divide between the Saxothuringian and Moldanubian units. Meanwhile, DAVA in the far south, reflects almost a N-NE trend in fast direction for all backazimuths, which corresponds to the direction of maximum stress due to collisional deformation of the Alps. WLF, the farthest west station, reflects two very different fast directions based on backazimuth. For events from 50° backazimuth, we observed the predicted NE-SW fast direction. However, for events from 250°, the fast direction is NW, similar to the strike of the nearby Lower Rhine Graben.

Unfortunately there is less information available for comparison for the northern stations of BSD, IBBN and MUD. BSD is quite close to a major NW-SE striking suture zone, which parallels the Tornquist-Teisseyre Zone. However, the fast direction recorded at this station is 33°, or very NE-SW trending, and almost seems to be perpendicular to this suture zone. Meanwhile, IBBN reflects a pattern unlike any of the other stations. It is sampling events from a backazimuth

of 250°, like many of the other stations, but the fast direction, -36°, does not agree with the NE trend expected in this western region. In fact, the fast direction here seems to almost parallel the Lower Rhine Graben, like WLF, though it is quite far away and in a different tectonic unit. BSD and MUD seem to reflect the larger transition from E-W to NW for fast directions from a backazimuth of around 250°, but there are additional events at MUD from a backazimuth of closer to 20° for which the fast direction is almost 90° off from this pattern.

With these results, we can begin to make some interpretations regarding how the observed anisotropy may correspond to surface features and subsurface deformation. Vinnik et al. (1994) claimed that the fast directions observed in this region are overwhelmingly perpendicular to the direction of maximum horizontal stress due to plate motion and thus anisotropy is a reflection of asthenospheric flow. However, Silver (1996) countered this argument, suggesting that this model of deformation could not capture the small-scale heterogeneity displayed in this region, in particular the rotation in the predominant fast direction from NE-SW in the east to NW-SE in the west. Similarly, the coherence of splitting parameters with surface structures provided further evidence for coupling between the crust and upper mantle and the fossilization of deformation as the primary source of anisotropy (Silver, 1996). Silver and Chan (1991) revised this position stating that strain due to asthenospheric flow is indeed *present* in these regions; however, internal deformation of the overriding plate is the *dominant* source of anisotropy. Montagner et al. (2000) found further evidence supporting this model, suggesting that the rapid variation in splitting parameters is likely a result of the assemblage of different tectonic units with different fossil anisotropic orientations. Our data, however, suggests that there may be multiple sources of anisotropy and thus a thorough characterization of subsurface structure in this region requires a combination of these different models.

4 RECEIVER FUNCTION ANALYSIS: Methods, Results and Interpretation

4.1 Methodology

Receiver function (RF) analysis is another popular method for characterizing subsurface structure, providing valuable vertical and geometrical constraints on anisotropy in the crust and upper mantle. RFs take advantage of Ps seismic phases that result from the conversion of P-waves into SV-waves (shear waves in the plane of motion) at velocity discontinuities. The largest Ps converted phase typically arises at the transition between the crust and mantle, known as the Moho, and thus RFs can be used to examine crustal structure and depth (Park and Levin, 2002). However, for a ray passing through a non-horizontal interface or an anisotropic layer, the effect of shear wave splitting will produce an additional, SH arrival on the transverse component (Wirth and Long, 2012; Wirth and Long, 2014). The variation of the amplitude and timing of the Ps arrival with backazimuth, coupled with the amplitude and polarity of Ps arrivals on the transverse component all provide information about the orientation and depth of discontinuities and helps distinguish dipping interfaces from anisotropic layers (Park and Levin, 2002; Wirth and Long, 2012; Wirth and Long, 2014;). It is expected that Ps energy on the transverse component will disappear at backazimuths parallel and perpendicular to the horizontal symmetry axis (Levin and Park, 1997).

A stacked receiver function is essentially a one-dimensional map of the structure below a seismic station, where the timing (known as the phase delay) and amplitude of Ps pulses are indicative of subsurface structure, namely the depth, strength and geometry of velocity contrasts and interfaces (Fouch and Rondenay, 2006). The method of building an RF consists of two major steps. The first step is data preprocessing, which includes the rotation of seismograms into the ray coordinate system of vertical (L), which contains mainly P energy, radial (Q), which should contain all P-S converted energy for the isotropic case, and transverse (T), which contains information about anisotropy or dipping interfaces. The second step combines deconvolution, inversion and stacking to improve the signal-to-noise ratio (Kind et al., 1995). Deconvolution is the process by which one separates the radial and transverse components, which contain the Ps signal, from the vertical component, which contains the bulk of the energy of the P-wave. This

distinguishes the event's source-time function from what is referred to as the ground's impulse response beneath the station (Park and Levin, 2002).

Despite some inherent limitations, Ps receiver function analysis is a useful tool for investigating receiver-side anisotropy. S-to-P RFs are also possible and, indeed, have the advantage that the Sp-wave arrives before the unconverted S-wave, which helps distinguish the converted and parent phases and prevents contamination from multiples (waves that have undergone additional reflections within the crust). However, with Sp phases, it is more difficult to differentiate the SV and SH wave and thus Ps receiver functions are more valuable for examining anisotropy specifically (Wirth and Long, 2014). With Ps receiver functions, it is possible to take into account the different paths taken by different phases in the mantle by migrating the receiver functions to different depths with a locally specific velocity model. RFs also provide excellent resolution of anisotropic structure at depth in a way that shear wave splitting cannot. Another advantage of Ps receiver function analysis is that it is relatively straightforward to distinguish between different causes of the P-to-SH conversion by examining backazimuthal variations in Ps polarity (Wirth and Long, 2014). For these reasons, Ps receiver functions are a valuable tool for characterizing subsurface processes that can provide constraints on anisotropy that are complementary to those provided by shear wave splitting analysis.

4.2 Methods and Data

In this study, we computed P-to-S receiver functions using the multi-taper correlation receiver function estimator of Park and Levin (2000), which estimates the correlation between horizontal and vertical component seismograms. We generated receiver functions for four long-running broadband stations in and around Germany, following the methodology of Wirth and Long (2012, 2014). Table 3 lists the stations used, along with their seismic network and length of their records. These stations were chosen from the original list of ten for which we had data after considering the complexity of the anisotropic pattern reflected in the shear wave splitting results, their relative locations in Germany, and the amount of data available. For station KHC, we had to discard data before 2003 as it had been recorded in a different format than the later data, at 15 samples per second, rather than the typical 20. We requested data for events with a magnitude

greater than 6.0 and an epicentral distance range of 20-100° and used a time duration for analysis of 80s.

Seismic Network	Station Code	Available Dates
Czech Regional Seismic Network (CZ)	KHC	2003-2015
Austrian Broadband Seismic Network (OE)	DAVA	2010-2014
Geofon Temporary Network (GE)	RUE	2000-2006
Geofon Temporary Network (GE)	STU	1994-2005

Table 3: Seismic network, station code, and dates of available data for the stations utilized in this receiver function analysis

We created two sets of both radial and transverse receiver functions at each station for three different values of frequency filter: 0.1, 1 and 2Hz. The first set ignored the effects of diverging raypaths at depths, while the second migrated the receiver functions every 20km from 0-160km. For the migration, we used a one-dimensional velocity model, 135, appropriate for continental settings (Kennet et al., 1995). The resulting RFs were stacked to help cancel out random noise. We produced both epicentral and backazimuthal RF swaths. The latter stack the data for all epicentral distances and then plot arrivals by backazimuth, plotting every 10°. The resulting radial RFs were used to calculate the depths of Ps conversions, while the transverse RFs were used for identifying anisotropy and dipping interfaces. The epicentral gathers stack by backazimuth and then plot arrivals by epicentral distance. We produced three epicentral gathers for each station, each for a limited swath of backazimuth, so we could ensure that the incoming waves were sampling the same structure. The backazimuthal increments were 0-80°, 135-210° and 255-330°. These epicentral gathers were crucial for identifying if a pulse was an actual conversion due to Earth structure or simply a multiple (e.g. Wirth and Long, 2012).

4.3 Results

We produced radial and transverse receiver functions stacked by both epicentral distance and backazimuth, as shown in Figures 10-14. The RFs low-passed with a frequency of 2Hz were noisy and thus we focused on the 0.5 and 1Hz RFs. Similarly, the migrations typically did not cause any significant changes to the RFs, though they did clean up some of the arrivals, so we

present here results obtained from the migrated RFs. In general, a positive polarity (blue) represents a velocity increase with depth, exemplified by the Moho, while a negative polarity (red) represents a velocity decrease with depth, such as the mid-lithospheric discontinuity. Below we describe the results obtained for each individual station along with our interpretation process.

We began the interpretation by identifying the Moho on the radial RF as an important element of subsurface structure. To do this we first estimated the arrival time of the strongest pulse (after the initial P-wave pulse at 0s). Then, assuming an average P-wave crustal velocity of 6.3kms^{-1} and a V_p/V_s ratio of 1.73, we calculated, using the method of Zhu and Kanamori (2000), that phase delay had to be multiplied by a factor of 8.4 in order to convert time to depth (Hrubcová and Geissler, 2009). We then used the epicentral gathers to determine whether other significant pulses on the radial RF were in fact conversions or simply multiples. To do this, we examined whether there was move-out (ie. increasing phase delay with increasing distance) of the arrival when plotted by epicenter (Wirth and Long, 2014). For a real Ps conversion, as distance increase we expect the phase delay (arrival time) to decrease because the raypath is more vertical. However, for a multiple, the phase delay will increase with distance because the wave reflects off the crust and thus spends more time as an S-wave. Near surface multiples must be accounted for in order to accurately characterize conversions due to anisotropy (e.g. Wirth and Long, 2014). The next step in the interpretation was to examine the polarity reversals on the transverse RFs for evidence of dipping layers or anisotropy. According to Levin and park (1997), anisotropy with a horizontal symmetry axis results in four polarity reversals across the full backazimuthal range, with no SH energy parallel and perpendicular to the axis of symmetry. In contrast, a dipping interface results in a two-lobed pattern, with no signal parallel to the dip of the boundary. A dipping anisotropic layer results in a mixture of two- and four- lobed polarity reversals (Wirth and Long, 2014).

KHC

The RFs produced for station KHC have good backazimuthal coverage, as one would expect given the length of the record. The migrated backazimuthal and epicentral gathers for the radial and transverse component, lowpassed at 0.5 and 1Hz are shown in Figure 10. On the radial RF, the first strong, positive-polarity arrival after the initial P-wave, which we interpret at the Moho,

is at approximately 4s. Using our multiplication factor of 8.4, this implies an approximate Moho depth of 34km. There is a very strong negative polarity pulse at 140° backazimuth that stretches across the time axis. Given how it diminishes at higher frequencies, we assumed that this was a remnant of noise in the data or an error in the processing procedure rather than an actual structure.

There is a strong negative polarity pulse at approximately 10s across the entire backazimuthal range. This translates to a depth of approximately 84km and is possible evidence of the mid-lithsopheric discontinuity. This sharp decrease in seismic velocity with depth is too shallow under continental interiors to demarcate the lithosphere-asthenosphere boundary, but it is a pervasive feature below continents that lacks an obvious cause or explanation (e.g. Abt et al., 2010; Wirth and Long, 2014; Selway et al., 2015). There is another noticeable positive polarity pulse at approximately 8s, translating to roughly 67km depth. This feature is even more obvious when the RFs are plotted by epicentral distance. Interestingly, while this feature has positive polarity at the backazimuthal range of 0-80°, it is weaker and negative from 255-330°. However, the arrival time of this pulse appears to get slightly later with increasing distance, suggesting that it is a multiple.

On the transverse component, it appears that there is possibly move-out in the signal, suggesting non-horizontal interfaces. There is what appears to be a two-lobed polarity reversal at approximately 12s with negative signal in the backazimuthal range from 70°-240°, though it is impossible to constrain this pattern precisely given the lack of data at intermediate backazimuths. At approximately 4s and 6s, there is a pattern of a curving interface, with a transition in polarity at the missing backazimuthal range. It is possible that these could be indicative of structural trends in polarity. For example, at 4s, it is conceivable that there is a four-lobed reversal with negative polarity up to at least 140° backazimuth and then again from roughly 210-230°.

Fig. 10 (next page): Migrated radial (left) and transverse (right) receiver functions for station KHC: Top left, backazimuthal gather filtered at 0.5Hz; Top right, backazimuthal gather filtered at 1Hz; Bottom left, epicentral gather for backazimuthal range 0-80 for frequency 0.5Hz; Bottom right, epicentral gather for backazimuthal ranger 255-210 for 0.5Hz filter. Negative polarities (red) indicate a velocity decrease with depth while positive polarities (blue) indicate a velocity increase with depth. If there were no anisotropic or dipping layers, there would not be any energy on the transverse RF.

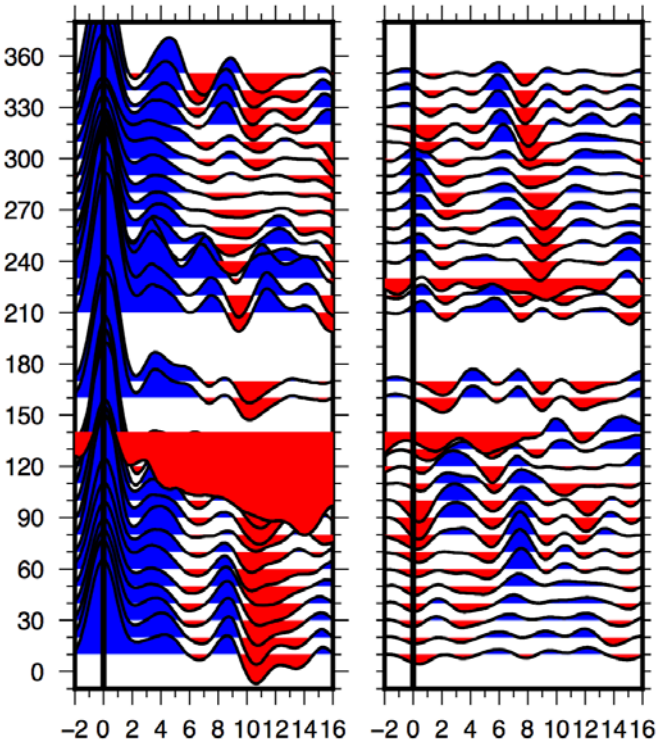
360
330
300
270
240
210
180
150
120
90
60
30
0
−2 0 2 4 6 8 10 12 14 16
−2 0 2 4 6 8 10 12 14 16

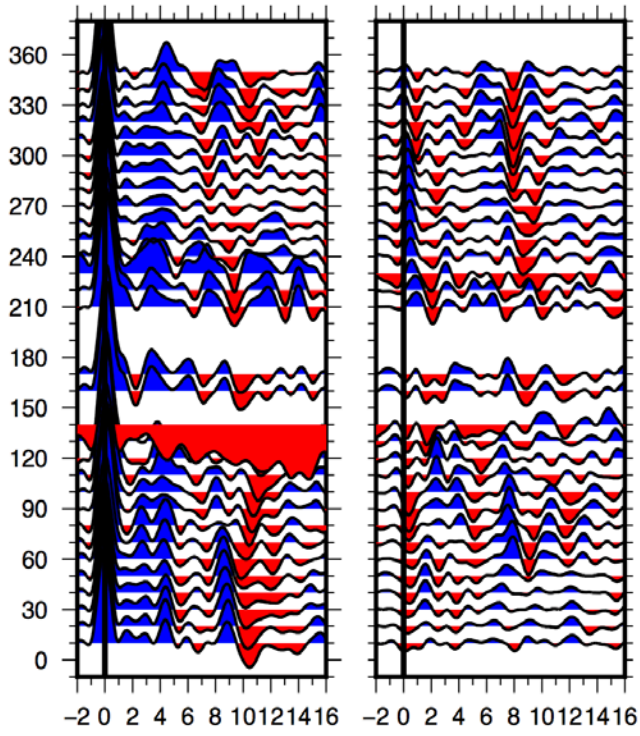
360
330
300
270
240
210
180
150
120
90
60
30
0
−2 0 2 4 6 8 10 12 14 16
−2 0 2 4 6 8 10 12 14 16

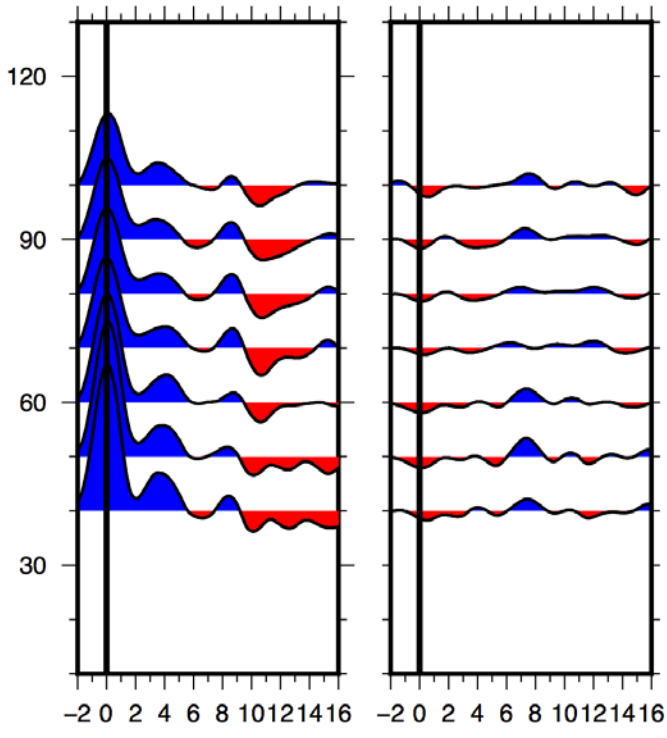
120
90
60
30
−2 0 2 4 6 8 10 12 14 16
−2 0 2 4 6 8 10 12 14 16

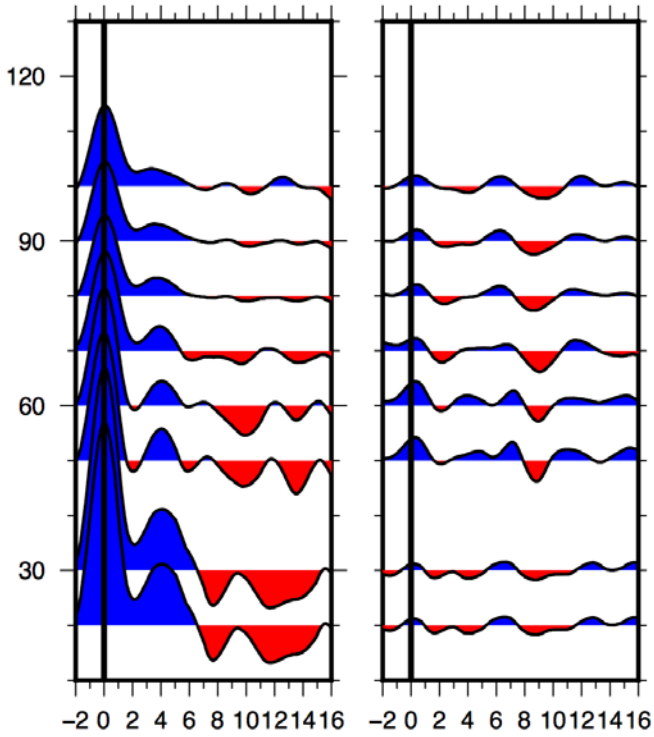
120
90
60
30
−2 0 2 4 6 8 10 12 14 16
−2 0 2 4 6 8 10 12 14 16

DAVA

The backazimuthal coverage at station DAVA is clearly not as complete as at KHC, given the lack of data between the backazimuths of 130° and 220°. The first phase arrival corresponding to the initial P-wave is slightly later here than at KHC, closer to 4.5s. The Moho is thus quite a bit deeper here at roughly 38km. There is a strong negative polarity at approximately 7s or 59km depth. However, unlike at KHC, this pulse is not clear across the entire backazimuthal range and could reflect the presence of noise. There is no positive polarity pulse observed at greater phase delay like at KHC. The migrated backazimuthal and epicentral gathers for the radial and transverse component, lowpassed at 0.5 and 1Hz are shown in Figure 11.

On the transverse component, it is difficult to identify two- and four-lobed polarity reversals because of the extent of the missing data at intermediate backazimuths. There are clearly polarity changes over that gap, but it is impossible to identify any precise patterns and thus accurately distinguish anisotropy from dipping interfaces or determine the geometry of these layers. However, at 3s there is clearly a two-lobed pattern, where there is a positive signal from 0-60° backazimuth, and from 240° on. Without the missing data we cannot put better constraints on the extent of the negative signal. There is a similar pattern at 13s, where there is no signal from 0-60° and from 270° onwards, but the basic problem of interpreting this pattern remains. There is a similar pattern at 5s and 9s, suggesting that there could be a four-lobed reversal depending on what is contained in that intermediate backazimuthal range.

Fig. 11 (next page): Migrated radial and transverse receiver functions for station DAVA: Top left, backazimuthal gather filtered at 0.5Hz; Top right, backazimuthal gather filtered at 1Hz; Bottom left, epicentral gather for backazimuthal range 0-80 for frequency 0.5Hz; Bottom right, epicentral gather for backazimuthal range 255-210 for 0.5Hz filter

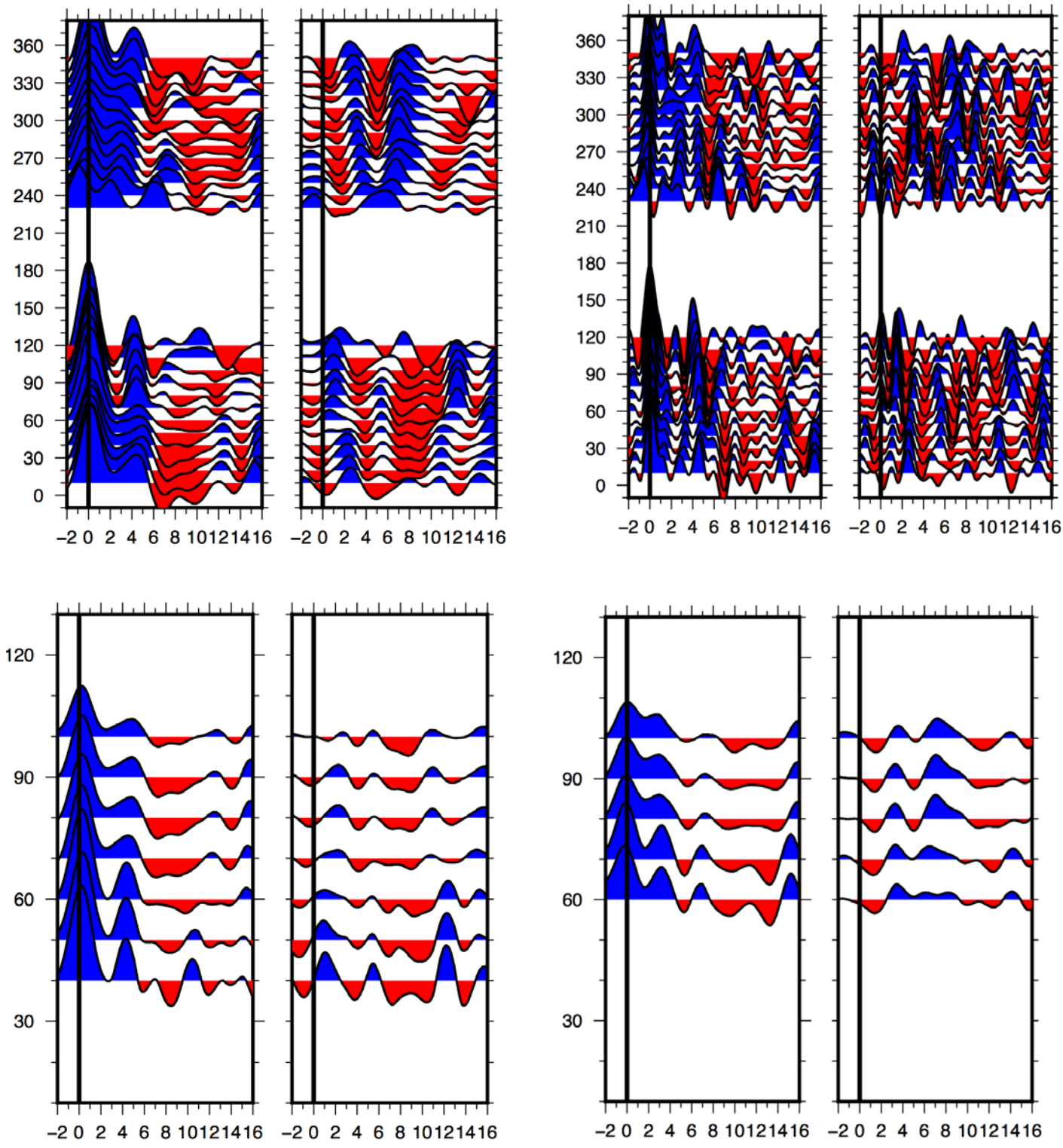

RUE

The backazimuthal coverage at station RUE is similar to that of DAVA, with no coverage between 130°-150° and 180°-250°. This is also the one station where there is a significant

difference between the migrated and unmigrated RFs. For this reason, we have included the unmigrated RF for comparison, lowpassed at a frequency of 0.5Hz in figure 12. The migration reduces the clarity and magnitude of the positive polarity pulses observed on the unmigrated RF at approximately 8s (68km) and 13s (109km). In fact, the migration appears to reverse the polarity of these pulses over swaths of the backazimuthal range. The migration also exaggerates a negative polarity pulse at approximately 15s, making it one of the dominant features on the RF, even when lowpassed at a higher frequency.

The arrival of the Ps phase converted at the Moho is far less clear at this station than the previous. At low frequency, there is a constant positive polarity at the beginning of the RF after the main P-arrival from 0-6s. This feature is resolved somewhat into three distinct peak when filtered at a higher frequency of 1Hz. It is difficult to constrain which peak exactly is the Moho, with possible phase delays of two to four seconds, corresponding to depth estimates of 17-33km. Just from what we known of the geology of this region, it is more likely that the Moho is at the lower end of this estimate, closer to 33km depth, and that the first pulse around 2s is perhaps due to reflections off of an interface within the crust. The receiver functions plotted by epicentral distance are displayed in figure 13.

On the unmigrated RF, we see, as with station KHC, a strong positive polarity pulse along the entire backazimuthal range at approximately 8s or 67km. This pulse is very obvious on the epicentral gathers, for all backazimuthal swaths. As with KHC, there is an interesting pattern in how that pulse appears on the epicentral gathers. For backazimuths of 255-330°, the phase delay increases with increasing distance, suggesting that this feature is a multiple. However, at 0-80° backazimuth, the phase delay appears to remain constant or even decrease with increasing distance, which would suggest that it is a real conversion. Unfortunately, this feature almost disappears after the migration. The other significant positive pulse at 13s is most certainly a multiple, displaying increasing phase delay with distance over the entire backazimuthal range. However, this feature also seems to disappear with the migration. Another obvious feature is the negative polarity pulse at ~15s, or 126km depth, that is amplified with the migration. This could potentially represent the mid-lithospheric discontinuity, though it is rather deep.

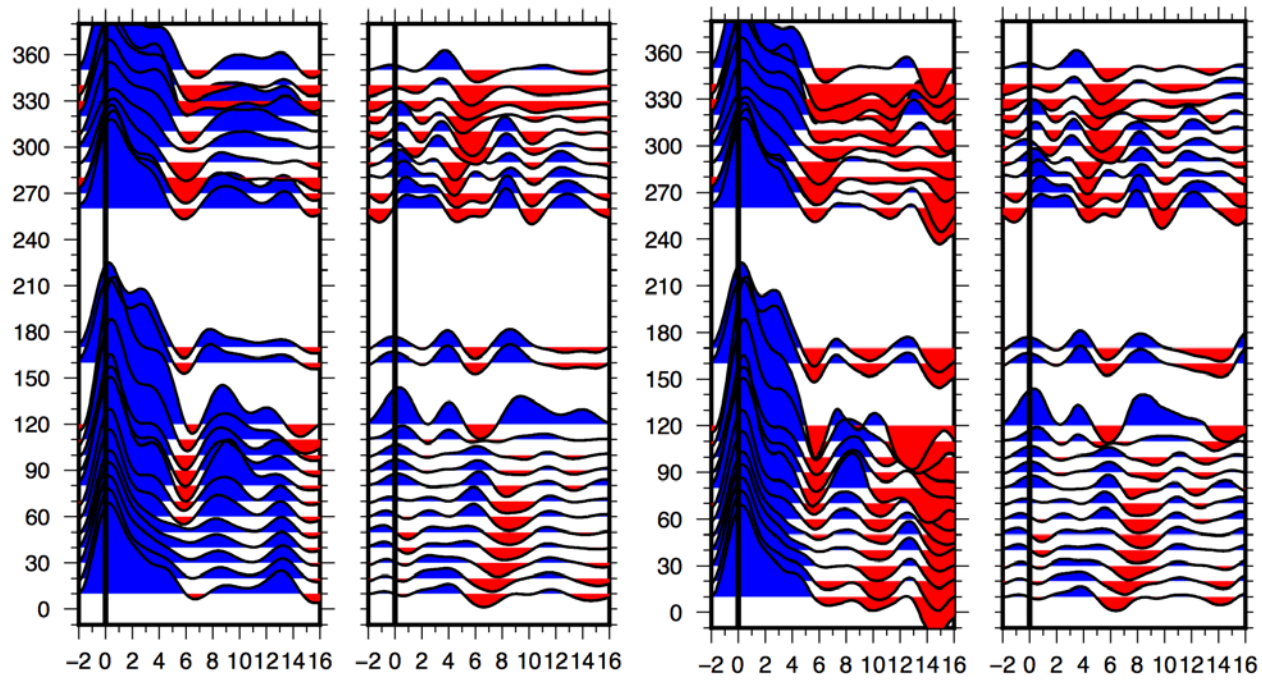

Fig. 12: Radial and transverse receiver functions for station RUE filtered at 0.5Hz: Left, unmigrated receiver function; Right, migrated to depth of 160km using velocity model AK135 (see section 4.2)

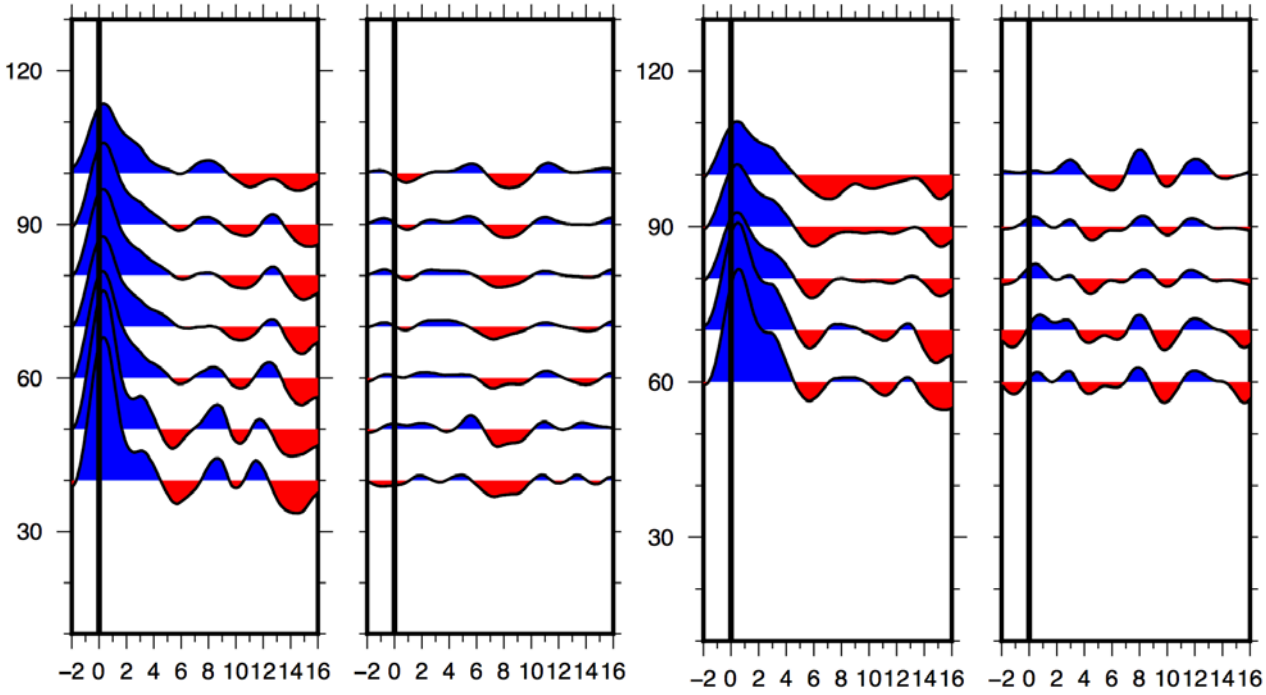

Fig. 13: Migrated radial and transverse receiver functions for station RUE stacked by backazimuth and plotted by epicentral distance for backazimuths 0-80 (left) and 255-310 (right) and filtered at 0.5Hz.

As with DAVA, there is a sufficient amount of backazimuthal coverage missing that precise interpretation of the transverse component RF is difficult. However, on the transverse component, it appears that there may be move out of arrivals, suggesting dipping interfaces, particularly around 6s. At approximately 2s, there appears to be a four-lobed polarity reversal with negative signal in the backazimuthal range of 90-260° and 300° onwards. There is also a possible two-lobed reversal at approximately 9s with no signal from 0-110° and 320° onwards. In addition, there is a clear transition from positive to negative polarity at approximately 12s, but it cannot be determined how this corresponds to structure without the missing backazimuthal coverage.

STU

STU has perhaps the best backazimuthal coverage of all four stations, with events only missing at the backazimuthal range of 130°-140° and 170°-190°. The migration, as with station RUE, amplifies a negative polarity pulse and weakens a positive pulse on the radial RF at approximately 13s and 10s, respectively. These are the only appreciable differences between the migrated and unmigrated RFs and the same basic features appear on both. The migrated backazimuthal and epicentral gathers for the radial and transverse component, lowpassed at 0.5 and 1Hz are shown in Figure 14.

As at station RUE, at low frequency, the initial P-arrival and the arrival of the phase likely converted at the Moho are joined. However, these peaks are clearly resolved when filtered at 1Hz, and the positive polarity pulse of the Moho is very clearly at 3s, or approximately 26km. As mentioned, there is a clear positive polarity pulse at approximately 10s, or roughly 84km, over the entire backazimuthal range. This feature is most certainly a multiple. There is also a very clear negative polarity pulse, amplified by the migration, at approximately 13s or 109km. This could be evidence of the MLD. Similarly, like RUE, STU displays significant curvature in the signal for individual arrivals, suggesting dipping interfaces, particularly around 6s.

Fig. 14 (next page): Migrated radial and transverse receiver functions for station STU: Top left, backazimuthal gather filtered at 0.5Hz; Top right, backazimuthal gather filtered at 1Hz; Bottom left, epicentral gather for backazimuthal range 0-80 for frequency 0.5Hz; Bottom right, epicentral gather for backazimuthal range 255-210 for 0.5Hz filter

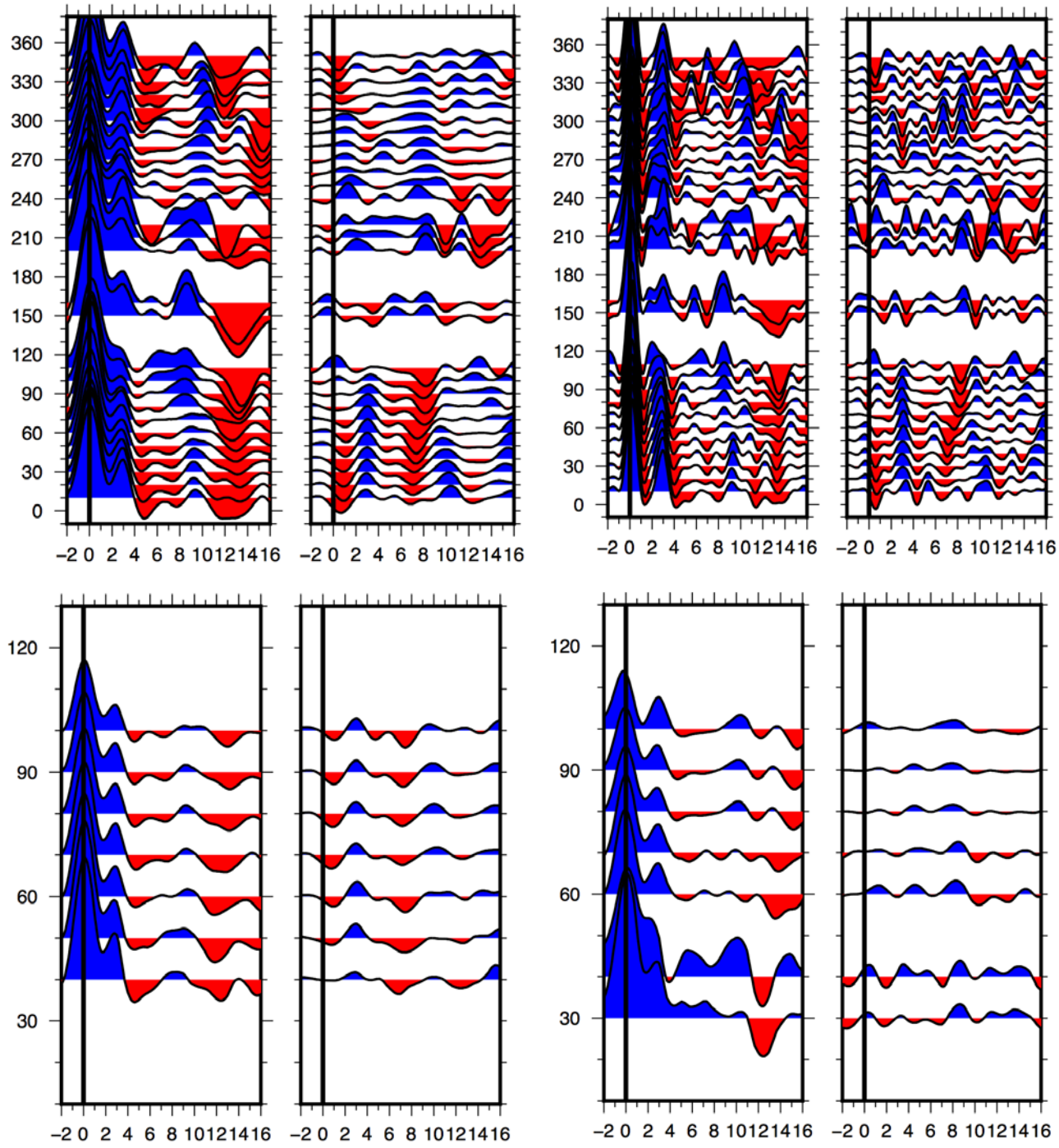

Identification of changing polarity patterns is simpler at STU, where there is better backazimuthal coverage. At approximately 1s, there is a two-lobed reversal with negative signal until at least 160° backazimuth and then from 310° onwards. There is a possible four-lobed

reversal at approximately 4s, around the depth of the Moho, with negative polarity from at least 150°-160°, and then again past roughly 270° backazimuth. There is a clear transition from negative to positive polarity at approximately 8s, but it is impossible to classify this pattern without greater backazimuthal coverage. There is also another possible four-lobed reversal at 11s with negative signal from 60°-220° backazimuth and then roughly 280° on.

4.4 Interpretation

In the same manner as our shear wave splitting analysis, we can compare the results of our receiver functions to previous studies that have calculated similar approximate Moho depths in and around Germany, as discussed in section 2.4. Zeis et al. (1990) estimated a depth of 35km for KHC, 39km for DAVA, and 27km for STU. In agreement to these results, Blundell et al. (1992) observed a band of shallow crust along a NE-SW trending band across the region and two deep crustal roots in the south and the northeast, estimating depths of roughly 38km depth for DAVA, 36km for KHC, 26km for STU and 32km for RUE. All of the studies that utilized receiver function analysis found that the largest Ps phase corresponded to a conversion off of the Moho, which was also the case in our data. Both STU and RUE displayed a double-peaked structure immediately following the primary P-arrival, but this feature was better resolved at higher frequencies allowing us to identify the likely Moho conversion. While our RFs were quite noisy, we can be confident of the larger features they display as our calculated Moho depths were within the range of previous studies. We calculated the depth of the Moho to be roughly 34km for KHC, 38km for DAVA, 33km for RUE, and 26km for STU, which are all approximately the same as estimated by previous studies.

In the RFs for all of our stations, despite the incomplete backazimuthal coverage at DAVA and RUE in particular, we were able to identify some notable positive and negative polarity pulses corresponding to velocity contrasts after the obvious Moho interface. DAVA was the only one that did not display any significant conversions across the entire backazimuthal range. Both STU and RUE had obvious multiples, identified because of the move out observed when plotted by epicentral distance, at 10s and 13s, respectively. KHC and RUE also each had a feature that was likely a multiple, but with an interesting pattern when plotted by epicentral distance. At KHC, at roughly 67km, there was a positive polarity pulse that displayed move out on the epicentral

gather typical of multiples in the backazimuthal range of 0-80°. However, in the range of 255-330° backazimuth, the pulse was far less noticeable and seems to transition into a negative polarity. Similarly, at RUE, also at 67km, there is a positive polarity pulse which is likely a multiple in the backazimuthal range 255-330°, but almost appears to be a real conversion (ie. phase delay decreases with increasing distance as one expects) from 0-80° backazimuth. These patterns could be products of noise or errors in data processing; however, they could be evidence of subsurface lateral heterogeneity. This would be not be surprising as we have already observed with shear wave splitting substantial variations in anisotropy and structure with backazimuth.

Each station also displayed a noticeable negative polarity pulse, which corresponds to a velocity decrease with depth. It was suggested that this might be evidence of the mid-lithospheric discontinuity. However, there is no obvious pattern regarding where this feature appears under each station and, with our multiplication factor for converting time to depth, it is deep enough at some stations to be the actual lithosphere-asthenosphere boundary. Geissler et al. (2010) found a typical continental lithosphere depth of 100km beneath most stations in Central Europe. The thickness was closer to 130km near the Trans-European Suture Zone in the northeast and 120km in the southwest part of the Bohemian Massif, towards the Alps. They also found a substantially thinner lithosphere of only 80km beneath the Upper Rhine Graben in the southwest. The negative pulse was observed at roughly 109km at STU, 126km at RUE, and 84km at KHC. There was also a pulse at DAVA at 59km, though it was not as strong across the entire backazimuthal range. STU is in the southwest part of the Bohemian Massif (Fig. 2) and thus an interface at 109km could potentially correspond to the actual lithosphere-asthenosphere boundary. It is interesting to note that STU displays a lithosphere thickness that is much higher than under the Upper Rhine Graben while the orientation of the fast direction at the station is relatively similar to the strike of that feature. RUE is quite close to the suture zones of the northeast and thus the conversion observed at 126km could also potentially represent the bottom of the lithosphere, rather than a mid-lithospheric interface. The interface at DAVA, at 59km, given how deep the lithosphere is estimated to be towards the Alps, is the only feature that could be interpreted as the MLD, though, as mentioned, the signal is not particularly strong.

Because of the relatively poor backazimuthal coverage it is difficult at some stations to precisely identify the two-lobed and four-lobed polarity reversal patterns corresponding to dipping and anisotropic layers, respectively. At KHC, there is a two-lobed reversal at approximately 100km with negative signal from 70-240°. No transverse energy is expected parallel to the orientation of the dipping interface; however, the lack of resolution at intermediate backazimuths prevents us from constraining the precise orientation of this layer with the available information. There is also a two-lobed pattern observed at STU at 8km and potentially 67km, at RUE at 76km and roughly 101km, and at DAVA at 25km and 109km. Though these depths and patterns are difficult to resolve, there is likely a dipping interface across much of the region around 105km and possibly around 70km and in the crust as well. The extent of negative signal, reflecting the orientation of the interface, varies quite dramatically between stations indicating that, if a dipping interface does exist at these depths, it is not a consistent structure across the region. There are also four-lobed reversals displayed in the RFs for all four stations, indicating the presence of anisotropy as our shear wave splitting analysis suggests. This includes some sort of structure in the crust itself- near the Moho at KHC and DAVA, around 17km at RUE and right below the Moho at STU- suggesting a potential source of anisotropy in the crust. This seems unlikely with the delay times we calculated, but, as with the splitting, it may be possible in light of the heterogeneity and complexity observed. There are also possible four lobed patterns around 76km at DAVA and 72km at STU. The backazimuthal variations of these polarity changes can be used to infer the orientation of dipping layers and the anisotropic symmetry axis.

Although we cannot precisely constrain the depth or orientation of the structures sampled in the receiver functions, the obvious combination of two- and four-lobed polarity reversals, as well as the curvature in the observed arrivals, suggests that the upper mantle in this region is highly layered and complex. There is certainly a combination of dipping interfaces and anisotropic layers, some of which likely have non-horizontal axes of symmetry. Similarly, the difference in the layering patterns between stations suggests that the subsurface is highly laterally heterogeneous. Figure 15 shows the migrated transverse component receiver functions, filtered at 0.5 and 1Hz, for each station. The extreme variability evident between each station and at different filters provides further evidence for dramatic lateral and horizontal heterogeneity. This complexity supports the conclusion that this continental region is a convoluted assemblage of

many different tectonic units and structures. Given these results it is also possible that the different groups of splits seen at different backazimuths in our splitting analysis are the results of anisotropy at different depths, which may help explain the backazimuthal variation in splitting parameters.

Fig. 15 (next page): Transverse component receiver functions, stacked by epicentral distance and plotted by backazimuth for each station, filtered at 0.5Hz (left) and 1Hz (right). Key to panels: Top left, KHC; Top right, DAVA; Bottom left, RUE; Bottom right, STU

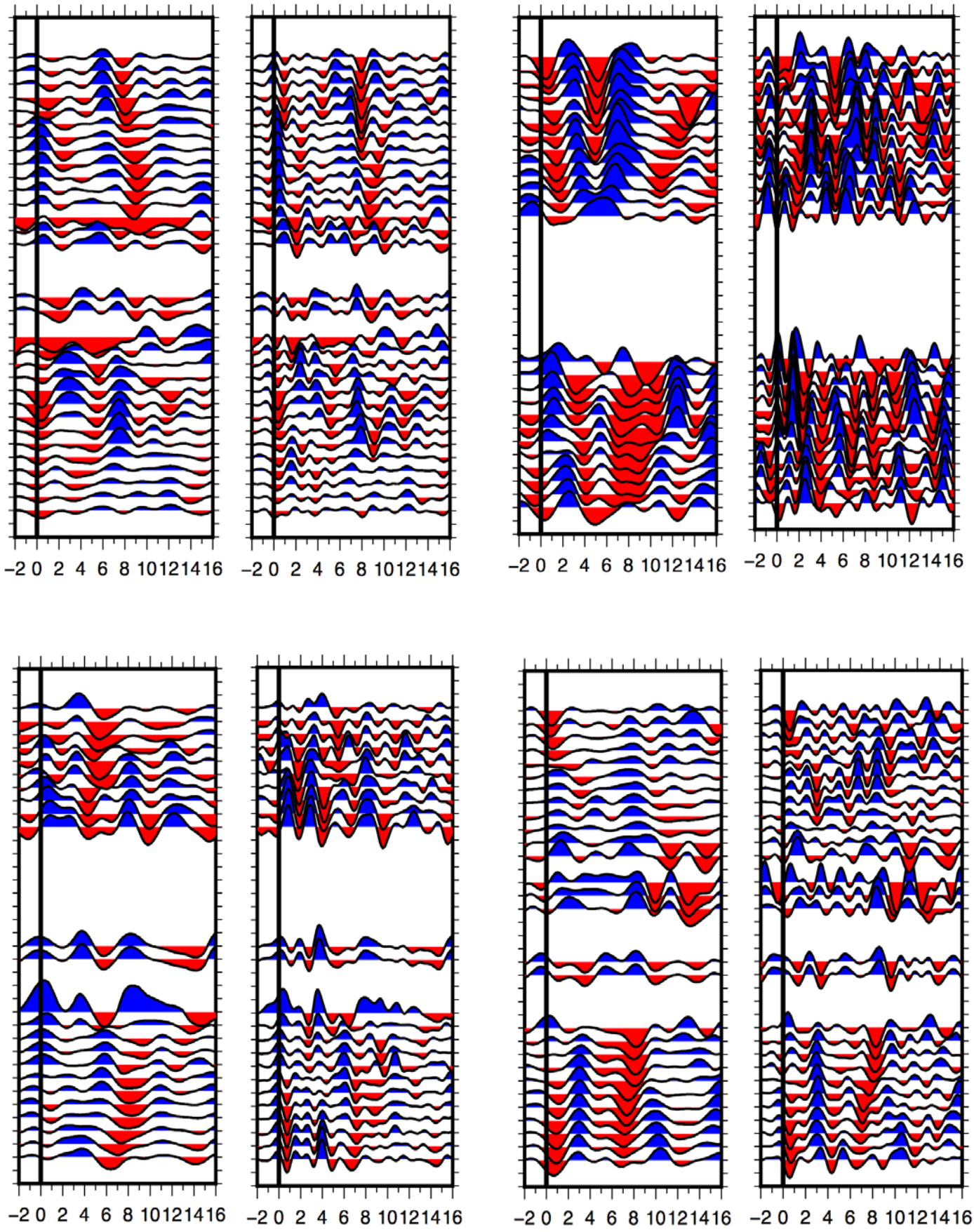
−2 0 2 4 6 8 10 12 14 16
−2 0 2 4 6 8 10 12 14 16
−2 0 2 4 6 8 10 12 14 16
−2 0 2 4 6 8 10 12 14 16
−2 0 2 4 6 8 10 12 14 16
−2 0 2 4 6 8 10 12 14 16
−2 0 2 4 6 8 10 12 14 16
−2 0 2 4 6 8 10 12 14 16

5 DISCUSSION

5.1 Evidence for Complex Anisotropic Structure

Liu and Gao (2013) point out that the literature is rife with discrepancies in observed anisotropic patterns at and around the same stations. This is in part due to changing techniques, improved computational power, and increased data availability. These factors are applicable in this region where many of the previous studies were done in the 1990s and early 2000s and characterized anisotropy via head wave velocity residuals, rather than shear wave splitting, and created receiver functions assuming isotropy to identify dipping interfaces, ignoring anisotropic signals. They also point out that many of the published results may simply have been determined incorrectly, particularly when calculations were done manually rather than with a computer. Both Long and van der Hilst (2005) and Liu and Gao (2013) note that discrepancies in observations, on the order of what we are observing in this study with past work, may potentially be a result of more complex and heterogeneous anisotropy. If most of the previous studies we have discussed assumed a single layer of anisotropy with a horizontal axis of symmetry, as many studies do, it would explain the variation in results, particularly in regard to delay time, as anisotropy in this region is clearly far more complex.

Recognizing complex anisotropy during the measurement stage is crucial for more precisely understanding and interpreting splitting results. It is also more difficult to constrain the delay times with complex anisotropy, which may explain the large variation of observed delay times across the study area. Generally, complexity can be identified by the presence of both two- and four-lobed polarity reversals on transverse component receiver functions and variations in shear wave-splitting parameters by backazimuth (Liu and Gao, 2013; Wirth and Long, 2014). In the latter case, the observed splitting parameters must be considered ‘apparent’ rather than inherent. For example, in a two-layered system where the backazimuth is parallel or perpendicular to the fast direction of the lower layer, the splitting results will only reflect the geometry of the upper layer. The complications arising from this complexity, as well as the noisiness of the data, helps explain the discrepancy in our results obtained through these different methods (Long and Silver, 2009; Liu and Gao, 2013).

There are two common forms of complex anisotropy that can be observed through shear wave splitting analysis. This includes anisotropy with a single-layered structure with a dipping axis of symmetry, which should display 180° periodicity in shear wave splitting results, and two layers with horizontal symmetry, which should present itself with 90° periodicity (Silver and Savage, 1994; Long and Silver, 2009; Liu and Gao, 2013). Both of those types seem evident in this data set, with variations in splitting parameters with backazimuth and depth at and between stations, though few stations display the characteristic periodicity predicted.

This complexity is further supported by our receiver function analysis, which suggests that anisotropy is depth dependent, and that there are multiple layers, producing different splitting parameters at different backazimuths. The combination of two- and four-lobed reversals, as well as the curvature observed in the signal of individual conversions, suggests that the anisotropic layers may have non-horizontal axes of symmetry. This could help explain why there was a preponderance of null measurements in our splitting analysis across a wide range of backazimuths. Given that the methods used in SKS splitting studies assume horizontal layering and that we are clearly observing dipping interfaces, many of the nulls could be indicative of non-horizontal anisotropic structure rather than isotropy.

The average delay time at these stations is far too large to be from crustal sources, given that Silver (1996) estimated that crustal anisotropy would produce delay times of only 0.1-0.3s and we are observing delay times up to 2.3s. However, there is clearly rapid lateral heterogeneity and some signal, according to the receiver functions, at crustal depths. Given that there are not major discrepancies at every station between SKS and SKKS event pairs, used as evidence of a contribution from the D" layer, it is therefore possible that we are observing some signal from heterogeneity in the crust. The complexity of anisotropy, in terms of the number and orientation of layers, may be complicating a simple interpretation of the source and deformation type responsible for the observed anisotropy. However, we can conclude that the anisotropic signature is dominated by fossil anisotropy from different tectonic events, while also reflecting a contribution from present-day asthenospheric flow. This combination of sources, with different

depths and timescales, explains the dramatic lateral and vertical heterogeneity and complex anisotropic signal, observed in this data.

5.2 Surface Wave Analysis

In addition to our analyses of shear wave splitting and receiver functions, we briefly anisotropic predictions based on surface wave models in order to further understand the advantages and limitations of available computational techniques. Surface waves propagate horizontally in the crust and upper mantle and are thus sensitive to structure at depths of approximately one-third the wavelength, providing different constraints on anisotropy than our other methods (Fouch and Rondenay, 2006). There are two types of anisotropy that are perceived from surface waves. The first, called radial anisotropy, results from the velocity discrepancy between Rayleigh (parallel to the propagation direction) and Love (perpendicular to propagation direction) waves. The second, known as azimuthal anisotropy, refers to the variation in surface wave, specifically Rayleigh wave, velocity by propagation direction (Montagner and Guillot, 2002; Fouch and Rondenay, 2006; Long and Becker, 2010). Measurements of quasi-Love waves that have been scattered into Rayleigh waves, due to lateral heterogeneities in anisotropy, provide further constraints on anisotropy in the upper mantle (Long and Becker, 2010). The models used in this study, DKP2005 (Debayle et al., 2005) and LH08 (Levedev and van der Hilst, 2008), use Rayleigh wave velocity discrepancies to constrain upper mantle structure.

The primary advantage of surface wave analysis is that it can provide strong vertical resolution and is consequently a useful complement to shear wave splitting and receiver function analysis (Fouch and Rondenay, 2006). Unfortunately, surface wave tomography loses sensitivity to variations in azimuthal anisotropy at depths beyond 200-300km (Marone and Romanowicz, 2007). In addition, surface waves, like receiver functions, cannot provide the sort of lateral constraints offered by shear wave splitting. Particularly in regions of poor coverage, the global tomographic models have a lateral resolution of hundreds of kilometers, limiting their applicability to tectonically complicated continental interiors (Babuska et al., 1993; Montagner and Guillot, 2002; Marone and Romanowicz, 2007; Long and Becker, 2010; Becker et al., 2012). Furthermore, similar to the receiver functions, one has to distinguish between potential causes of

particular patterns observed in the models as both lateral isotropic heterogeneity and anisotropy can produce the same first-order signal (Fouch and Rondenay, 2006).

Nevertheless, despite its limitations, it is useful to preform even a cursory analysis of surface wave models in this region as a point of comparison for our other techniques. A longstanding question in this field has been the often-conflicting observations of anisotropy obtained from shear wave splitting measurements versus surface wave modeling (Long and Becker, 2010). Montagner et al. (2000) were some of the first to compare splitting observations from shear waves, measured by Silver (1996), with predictions of anisotropy made by Montagner and Tanimoto (1991) on a global scale. However, this study and those that followed rarely observed a match in their results. In complex continental interiors, such comparisons very often disagree, particularly at a regional scale (Debayle et al., 2005; Long and Becker, 2010). This disagreement is not surprising given the different lateral and vertical sampling scale and coverage of body waves versus surface waves (Long and Becker, 2010). For example, delay times are typically under-predicted, often dramatically so, by tomography in part because surface waves are unable to capture the potential contributions to anisotropy made in the deep mantle and transition zone (Becker et al., 2012). There has been better association between observations and predictions in ocean basins and tectonically active continental regions where large-scale tectonic processes are taking place. This is because of the homogeneity and consistency in subsurface structure in such regions versus in continental interiors, which are assemblages of smaller, independent tectonic blocks. The dimensions of these blocks are often less that of the wavelength of a surface wave, particularly in a geologically complex continent like Europe, and thus cannot be adequately sampled by surface waves alone (Montagner et al., 2000; Montagner and Guillot, 2002). For these reasons, surface wave analysis is most useful for resolving large-scale patterns of anisotropy due to more coherent processes like asthenospheric flow due to plate motion (Becker et al., 2012).

Figure 16, reproduced from Campbell et al. (2013), displays the splitting parameters predicted by the surface wave models of Debayle et al. (2005) and Levedev and van der Hilst (2008), as well as their backazimuthal coverage. The most obvious result is that the two models produce drastically different predictions of splitting in this region. For the backazimuths of approximately

45° and 250°, from which most of our results were obtained, Debayle et al. (2005) predicts a fast direction of approximately 90° and delay times of 0.2 and 0.3s, respectively. In contrast, Lebedev and van der Hilst (2009), for the same backazimuths, predict fast directions of 30° and 40° and delay times of 0.5s and 0.7s. For these same backazimuths across our stations, we observe an average fast direction of close to 90°, but delay times of 1.5s and 1.2s. More noticeably, our data lacks the approximately 90° periodicity, which would suggest two interfering layers of anisotropy, predicted by both surface wave models.

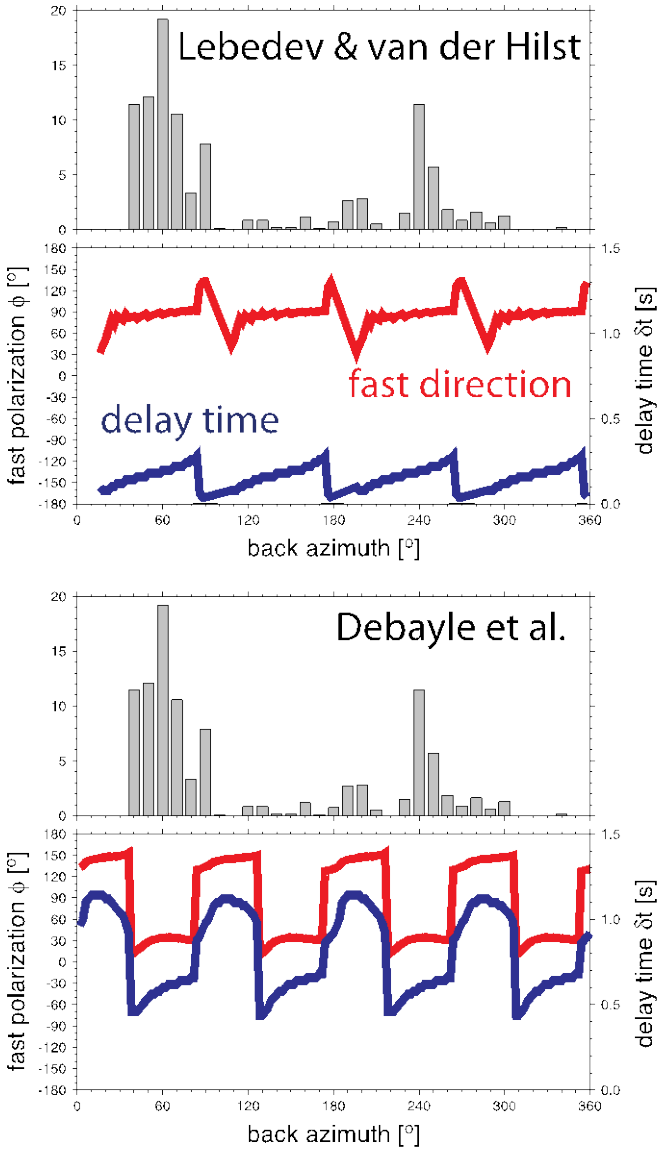

Fig. 16: Predictions of splitting parameters determined by the surface wave models of and Lebedev and van der Hilst, 2008 (top) and Debayle et al., 2009 (bottom). The top panel reflects the backazimuthal coverage of their measurements while the bottom panel reflects predicted parameters.

The results from our receiver function analysis provide a possible explanation for the discrepancies between our observed splitting parameters and these surface wave model predictions. The RFs indicate that anisotropy is highly variable laterally and vertically, on relatively short length scales. Given the wavelength of surface waves, they are simply not sensitive to the scales of heterogeneity observed in this study area. A regionally averaged model cannot capture the complexity we observe in anisotropy between stations in Germany. Perhaps a more regionally specific surface wave model can better capture the complexity in this region; however, the characteristic wavelength may still be too long to sample all of the structure evident in this region.

6 CONCLUSIONS AND FUTURE WORK

Measurements of *KS splitting and receiver function analysis indicates the presence of complex anisotropy beneath Germany and the surrounding region. Evidence from shear wave splitting suggests that there is significant lateral heterogeneity in this region, with splitting parameters varying dramatically between stations and at individual stations with backazimuth. Furthermore, we observe stark discrepancies between our results and those obtained from previous studies of anisotropy in this region. While our study has the advantage of more extensive data coverage, complexity is likely the primary reason behind these differences. We observe some association between observed fast directions and the strikes of surface geological features, suggesting some contribution to anisotropy from fossilized deformation in the upper mantle. However, deviations from this relationship suggest there is another source of anisotropy, perhaps from present-day asthenospheric flow due to plate motion.

Our receiver function analysis confirms the presence of complex anisotropy. We observe curvature in the phase delay of Ps conversion, as well as a combination of two- and four-lobed polarity reversals, which provides evidence for both dipping interfaces and anisotropic layers, as well as potential anisotropic layers with non-horizontal axes of symmetry. This helps explain the preponderance of nulls and the backazimuthal variations in our splitting measurements. We are able to use these results to identify and possibly explain discrepancies between our observations and predictions of anisotropic structure from surface wave tomographic models. It appears that the length scale of heterogeneity in this region is far less than what can be sampled by surface waves. We conclude that anisotropy in this region is laterally and vertically heterogeneous, reflecting a variety of different deformation processes in the mantle.

There are a variety of avenues for future work that should be pursued in order to build upon and improve the work presented here. Perhaps the most important and valuable opportunity is forward modeling of our receiver function data to better constrain our results in terms of the precise structure. In this technique, one builds synthetic receiver functions, manually adjusting the anisotropic parameters and geometry of subsurface layering in the model in order to recreate the observed data (Fouch and Rondenay, 2006; Wirth and Long, 2014). This will be difficult

given the complexity in this region, but it will allow us to better constrain the patterns reflected in the data, helping distinguish dipping interfaces from anisotropic layers and determine the thickness, strength, and orientation of those layers. We can also utilize a more regionally specific surface wave model to determine if that improves the association between the predictions and observations of shear wave splitting. A regionally specific model should be more sensitive to the heterogeneity observed in this data, laterally and with depth, and thus may allow us to put further constraints on the depth distribution of anisotropy. In addition, more work could be done to identify any discrepancies in SKS-SKKS event pairs in order to better understand the contributions to anisotropy from the lower mantle. While our study has clearly illustrated the extent of anisotropic complexity in this region, much more work will be required to precisely elucidate its causes and implications for continental development in central Europe.

ACKNOWLEDGEMENTS

First and foremost, I would like to thank my adviser, Maureen Long, who has been an extremely helpful, patient and kind adviser for almost four years now. This project, and most of my science exploits through college, would not have been possible without her! I would also like to thank Erin Wirth at the University of Washington, whose guidance was utterly invaluable for the work in receiver function analysis. I am also grateful to my collaborators, Sergei Lebedev at the Dublin Institute for Advanced Studies and Thorsten Becker at USC, for providing the surface wave predictions and to Colton Lynner for helping produce the GMT maps presented here. The seismic data used for this study was acquired through the IRIS Data Management Center and BGR's Observatories and Research Facilities for European Seismology from the following seismic networks: the Czech Regional Seismic Network, the Danish National Seismic Network, the Austrian Broadband Seismic Network, the German Regional Seismic Network, and the GEOFON Temporary Network. Further thanks are due to Andres Wüstfeld, Vadim Levin and Jeffrey Park for providing many of the scripts and software packages used in this study.

REFERENCES

Abt, D., Fischer, K., French, S., Ford, H., Yuan, H. and B. Romanowicz (2010). North American lithospheric disctontinuity structure imaged by Ps and Sp receiver functions. *Journal of Geophysical Research* **115**

Babuska, V., Plomerová, J and J. Síleny (1993). Models of seismic anisotropy in the deep continental lithosphere. *Physics of the Earth and Planetary Interiors* **78**: 167-191

Bamford, D. (1977). Pn velocity anisotropy in a continental upper mantle. *Geophysics Journal International* **49** (1): 29-48

Becker, T.W., Lebedev, S. and M.D. Long (2012). On the relationship between azimuthal anisotropy from shear wave splitting and surface wave tomography. *Journal of Geophysical Research* **117**

Blundell, B., Freeman, R. and S. Mueller. *A Continent Revealed: The European Geotraverse.* Cambridge University Press: Cambridge, 1992

Bormann, P., Burghardt, P.T., Makeyeva, L.I. and L.P. Vinnik (1993). Teleseismic shear-wave splitting and deformations in Central Europe. *Physics of the Earth and Planetary Interiors* **78**: 157-166

Bormann, P., Grünthal, G., Kind, R. and H. Montag (1996). Upper mantle anisotropy beneath central Europe from SKS wave splitting: Effects of absolute plate motion and lithosphere-asthenosphere boundary topography? *Journal of Geodynamics* **22** (1): 11-32

Campbell, L., Long, M.D., Becker, T.W. and S. Lebedev (2013). Complex seismic anisotropy beneath Germany from shear wave splitting and surface wave models. *AGU 2013 Fall Meeting Abstract* **DI11A-2161**

Debayle, E., B. L. N. Kennett, and K. Priestley (2005). Global azimuthal seismic anisotropy and the unique plate-motion deformation of Australia. *Nature* **433**: 509–512

Eakin, C.M., Long, M.D., Wagner, L.S. and S. L. Beck (2015). Upper mantle anisotropy beneath Peru from SKS splitting: Constraints on flat slab dynamics and interaction with the Nazca Ridge. *Earth and Planetary Science Letters* **412**: 152-162

Enderle, U., Mechie, J., Sobolev, S. and K. Fuchs (1996). Seismic anisotropy within the uppermost mantle of southern Germany. *Geophysics Journal International* **125**: 747-767

Fouch, M.J. and S. Rondenay (2006). Seismic anisotropy beneath stable continental interiors. *Physics of the Earth and Planetary Interiors* **158**: 292-320

Fuchs, K. (1983). Recently formed elastic anisotropy and petrological models of the continental subcrustal lithosphere in southern Germany. *Physics of the Earth and Planetary Interiors* **31**: 93-118

Geissler, W., Sodoudi, F. and R. Kind (2010). Thickness of the central and eastern European lithosphere as seen by S receiver functions. *Geophysics Journal International* **181 (2)**: 604-634

Grünthal, P. and D. Stromeyer (1992). The recent crustal stress field in Central Europe: trajectories and finite element modeling. *Journal of Geophysical Research* **97**: 11805-11820

Hrubcová, P. and W. Geissler (2009). The Crust-Mantle Transition and the Moho Beneath the Vogtland/ West Bohemian Region in the light of different seismic methods. *Studia Geophysica et Geodaetica* **53** (3): 275-294

Iturrino, G., Christensen, N., Kirby, S. and M. Salisbury (1991). Seismic Velocities and Elastic Properties of Oceanic Gabbroic Rocks from Hole 735B. *Proceedings of the Ocean Drilling Program, Scientific Results* **118**: 227-244.

Karato, S., Jung, H., Katayama, I. and P. Skemer (2008). Geodynamic Significant of Seismic Anisotropy of the Upper Mantle: New Insights from Laboratory Studies. *Earth and Planetary Sciences* **36**: 59-95.

Kennett, B.L.N., Engdahl, E.R., and R. Buland (1995). Constraints on seismic velocities in the Earth from travel times. *Geophysical Journal International* **122**: 108-124

Kind, R., Kosarev, G.L. and N.V. Petersen (1995). Receiver functions at the stations of the German Regional Seismic Network (GRSN). *Geophysics Journal International* **121**: 191-201

Lebedev, S., and R. D. van der Hilst (2008), Global upper-mantle tomography with the automated multimode inversion of surface and S-wave forms. *Geophysics Journal International* **173**: 505-518

Levin, V., and J. Park (1997). P-SH conversions in a flat-layered medium with anisotropy of arbitrary orientation. *Geophysical Journal International* **131**: 253-266

Liu, K., Gao, S. (2013). Making Reliable Shear-Wave Splitting Measurements. *Bulletin of the Seismological Society of America* **103** (5)

Long, M.D. (2009). Azimuthal anisotropy in D" beneath the eastern Pacific from SKS-SKKS splitting discrepancies. *Earth and Planetary Science Letters* **285**: 181-189

Long, M.D., Becker, T. W. (2010). Mantle Dynamics and Seismic Anisotropy. *Earth and Planetary Science Letters* **297**: 341-354

Long, M.D. and P.G. Silver (2009). Shear wave splitting and mantle anisotropy: Measurements, interpretations and new directions. *Survey of Geophysics* **30**: 407-461

Long, M.D. and R.D. van der Hilst (2005). Estimating shear-wave splitting parameters from broadband recordings in Japan: A comparison of three methods. *Bulletin of the Seismological Society of America* **95**: 1346-1358

Luschen, E., Nolte, B. and K. Fuchs (1990). Shear-wave evidence for an anisotropic lower crust beneath the Black Forest, southwest Germany. *Tectonophysics* **173**: 483-493

Makeyeva, L ., Plesinger, A . and J. Horâlek (1990). Azimuthal anisotropy beneath the Bohemian Massif from broad-band seismograms of SKS waves. *Physics of the Earth and Planetary Interiors* **62**: 298-306

Marone, F. and B. Romanowicz (2007). The depth distribution of azimuthal anisotropy in the continental upper mantle. *Nature* **447**: 198-201

Montagner J., Griot-Pommera, D. and J. Lavé (2000). How to relate body wave and surface wave anisotropy? *Journal of Geophysical Research* **105**: 19015-19027

Montagner, J. and L. Guillot (2002). Seismic Anisotropy and Global Geodynamics. *Reviews in Mineralogy and Geochemistry* **51**: 353-385

Montagner, J. and T. Tanimoto (1991). Global upper mantle tomography of seismic velocities and anisotropies. *Journal of Geophysical Research* **96**: 20337-20351

Nicolas, A. and N. Christensen (1987). Formation of Anisotropy in Upper Mantle Peridotites- A Review. *American Geophysical Union Geodynamics Series* **16**: 111-123

Park, J. and V. Levin (2000). Receiver functions from multiple-taper spectral correlation estimates. *Bulletin of the Seismological Society of America* **90**: 1507-1520

Park, J. and V. Levin (2002). Seismic anisotropy: Tracing Plate Dynamics in the Mantle. *Science* **296**: 485-489

Plenefisch, T. and K.P. Bonjer (1994). The stress tensor in the Rhine Graben area derived from earthquake focal mechanism (extended abstract). *Geologie Mijnbouw* **4**: 1-4

Savage, M. (1999). Seismic Anisotropy and Mantle Deformation: What Have We Learned from Shear Wave Splitting? *Reviews of Geophysics* **37** (1): 65-106

Selway, K., Ford, H. and P. Keleman (2015). The seismic mid-lithospheric discontinuity. *Earth and Planetary Science Letters* **414**: 45-57

Silver, P. (1996). Seismic anisotropy beneath the continents: Probing the depths of geology. *Annual Review of Earth and Planetary Sciences* **24**: 385-432

Silver, P.G. and W. W. Chan (1988). Implications for continental structure and evolution from seismic anisotropy. *Nature* **335**: 34-39

Silver, P. and W.W. Chan (1991). Shear wave splitting and subcontinental mantle deformation. *Journal of Geophysical Research* **96**: 16429-16454

Silver, P.G. and M.K. Savage (1994). The interpretation of shear-wave splitting parameters in the presence of two anisotropic layers. *Geophysics Journal International* **119**: 949-963

Sundberg, M. and R.F. Cooper (2008). Crystallographic preferred orientation produced by diffusional creep of harzburgite: Effects of chemical interactions among phases during plastic flow. *Journal of Geophysical Research* **113**

Vinnik L.P., Kosarev, G.L. and L.I. Makeyeva (1984). Anisotropy in the lithosphere from observations of SKS and SKKS (in Russian). *Dokl. Acad. Nauk SSSR* **278**: 1335-1339

Vinnik, L.P., Krishna, V.G., Kind, R., Bormann, P. and K. Stammler (1994). Shear wave splitting in the records of the German Regional Seismic Network. *Geophysical Research Letters* **21** (6): 457-460

Vinnik, L.P., Makeyeva, L.I., Milev, A. and Y. Usenko (1992). Global patterns of azimuthal anisotropy and deformation in the continental mantle. *Geophysics Journal International* **111**: 433-447

Winchester, J.A., Pharaoh, T.C. and J. Verniers (2002). Paleozoic Amalgamation of Central Europe. *Geology Society of London Special Publications* **201**: 1-18

Wirth, E.A. and M.D. Long (2012). Multiple layers of seismic anisotropy and a low-velocity region in the mantle wedge beneath Japan: Evidence from teleseismic receiver functions. *Geochemistry Geophysics Geosystems* **13**

Wirth, E. A. and M.D. Long (2014). A contrast in anisotropy across mid-lithospheric discontinuities beneath the central United States- a relic of craton formation. *Geology* **42** (10): 851-854

Wüstefeld, A. and G. Bokelmann (2006). Null Detection in Shear-Wave Splitting Measurements. *Bulletin of the Seismological Society of America* **97** (4): 1204-1211

Wüstfeld, A., Bokelmann, G., Zaroli, C. and G. Barruol (2008). SplitLab: A Shear-Wave Splitting Environment in Matlab. *Computers and Geoscience* **34**: 515-528

Wylegalla, K., Bormann, P. and M. Baumbach (1988). Investigation of inhomogeneities and anisotropy in the crust and upper mantle of Central Europe by means of teleseismic P waves. *Physics of the Earth and Planetary Interiors* **51**: 169-178

Zeis, S., Gajewski, D. and C. Prodehl (1990). Crustal structure of southern Germany from seismic refraction data. *Tectonophysics* **176**: 59-86

Zhu, L. and H. Kanamori (2000). Moho depth variation in southern California from teleseismic receiver functions. *Journal of Geophysical Research* **105**: 2969-2980